REPORT DOCUMENTATION PAGE

1. Recipient's Reference	2. Originator's Reference	3. Further Reference	4. Security Classification of Document
	AGARD-R-749	ISBN 92-835-0425-9	UNCLASSIFIED

5. Originator	Advisory Group for Aerospace Research and Development North Atlantic Treaty Organization 7 rue Ancelle, 92200 Neuilly sur Seine, France

6. Title	FUTURE RESEARCH ON TRANSONIC UNSTEADY AERODYNAMICS AND ITS AEROELASTIC APPLICATIONS

7. Presented at	the 63rd Meeting of the Structures and Materials Panel of AGARD, in Athens, Greece, 28 September—3 October 1986.

8. Author(s)/Editor(s)	9. Date
Various	August 1987

10. Author's/Editor's Address	11. Pages
Various	44

12. Distribution Statement	This document is distributed in accordance with AGARD policies and regulations, which are outlined on the Outside Back Covers of all AGARD publications.

13. Keywords/Descriptors

Transonic characteristics	Flutter
Unsteady state	Mathematical prediction
Aerodynamics	Aeroelasticity

14. Abstract

This Workshop focused on strategies for promoting and developing engineering-level transonic flutter prediction techniques.

The technology of transonic aerodynamics is currently undergoing rapid development. Significant progress is being made to solve the inherently nonlinear equations describing unsteady motions of wings in transonic flow, while the availability of reliable and efficient computational methods will greatly enhance the ability to predict the aeroelastic behaviour of modern aircraft operating under transonic flow conditions.

AGARD-SMP has previously coordinated unsteady aerodynamic research carried out on a number of "standard" wind tunnel model configurations and published the results. The proposals contained in the Evaluation Report (W.J.Mykytow) on the Fall 1984 Structures and Materials Panel Specialists' Meeting on "Transonic Unsteady Aerodynamics", together with an expanded range of aeroelastic configurations, formed the guidelines which this Workshop followed.

Two of the keynote papers presented at this Workshop are published in this Report.

AGARD-R-749

AGARD

ADVISORY GROUP FOR AEROSPACE RESEARCH & DEVELOPMENT

Paris.

7 RUE ANCELLE 92200 NEUILLY SUR SEINE FRANCE

AGARD REPORT No.749

Future Research on Transonic Unsteady Aerodynamics and its Aeroelastic Applications

AUGUST 1987

NORTH ATLANTIC TREATY ORGANIZATION

**DISTRIBUTION AND AVAILABILITY
ON BACK COVER**

NORTH ATLANTIC TREATY ORGANIZATION

ADVISORY GROUP FOR AEROSPACE RESEARCH AND DEVELOPMENT

(ORGANISATION DU TRAITE DE L'ATLANTIQUE NORD)

AGARD Report No.749

FUTURE RESEARCH ON TRANSONIC UNSTEADY AERODYNAMICS AND ITS

AEROELASTIC APPLICATIONS

THE MISSION OF AGARD

The mission of AGARD is to bring together the leading personalities of the NATO nations in the fields of science and technology relating to aerospace for the following purposes:

— Exchanging of scientific and technical information;

— Continuously stimulating advances in the aerospace sciences relevant to strengthening the common defence posture;

— Improving the co-operation among member nations in aerospace research and development;

— Providing scientific and technical advice and assistance to the Military Committee in the field of aerospace research and development (with particular regard to its military application);

— Rendering scientific and technical assistance, as requested, to other NATO bodies and to member nations in connection with research and development problems in the aerospace field;

— Providing assistance to member nations for the purpose of increasing their scientific and technical potential;

— Recommending effective ways for the member nations to use their research and development capabilities for the common benefit of the NATO community.

The highest authority within AGARD is the National Delegates Board consisting of officially appointed senior representatives from each member nation. The mission of AGARD is carried out through the Panels which are composed of experts appointed by the National Delegates, the Consultant and Exchange Programme and the Aerospace Applications Studies Programme. The results of AGARD work are reported to the member nations and the NATO Authorities through the AGARD series of publications of which this is one.

Participation in AGARD activities is by invitation only and is normally limited to citizens of the NATO nations.

The content of this publication has been reproduced
directly from material supplied by AGARD or the authors.

Published August 1987

PREFACE

The technology of transonic aerodynamics is currently undergoing rapid development. Significant progress is being made to solve the inherently nonlinear equations describing unsteady motions of wings in transonic flow, while the availability of reliable and efficient computational methods will greatly enhance the ability to predict the aeroelastic behaviour of modern aircraft operating under transonic flow conditions.

Calculation of the motion-induced unsteady airloads on oscillating wings in transonic flow requires large computer storage capacity and long computing times. Several computation techniques involving various degrees of approximation have been elaborated and are now available for use. However, it is difficult to compare and evaluate all these competing methods with regard to their applicability for economic, engineering-type aeroelastic predictions. Indeed, from the relatively simple Transonic Small Perturbation (TSP) equation up to the Full Potential Euler and Navier-Stokes Equations, a wide range of unsteady transonic flow prediction capabilities exists which apply finite difference, finite element and integral equation techniques, the results of which are manifested not only in computational accuracy but also in large differences of computing time and computer requirements. This was clearly demonstrated at the first AGARD-SMP Specialists' Meeting on "Unsteady Airloads in Separated and Transonic Flow" held in Lisbon, Portugal, in April 1977. At its subsequent fall 1977 meeting, the AGARD-SMP then formed a working group on "Standard Configurations for Aeroelastic Applications of Transonic Unsteady Aerodynamics" with members of six NATO countries under the auspices of the Subcommittee on Aeroelasticity. The aim of this working group was to accelerate — in a cooperative program — the development of new theoretical, numerical and experimental techniques in transonic unsteady aerodynamics and their application to aeroelastic problems of aircraft loads, stability and flutter. Based on the recommendations obtained by the members of this working group from aeroelasticians and aerodynamicists in their respective countries, a limited set of two-dimensional and three-dimensional aeroelastic configurations was defined as standard airfoils and wings, and a compendium of unsteady aerodynamic measurements in the transonic flow regime was elaborated.

After AGARD had established these standard configurations, the next step was to request aeroelasticians in the NATO countries to evaluate their methods. This effort culminated in a Specialists' Meeting on "Transonic Unsteady Aerodynamics and Its Aeroelastic Applications" held at the SMP fall 1984 meeting in Toulouse. This meeting clearly demonstrated that the AGARD cooperative program on transonic unsteady aerodynamics and aeroelastic applications has indeed stimulated excellent contributions to advance the state of the art which has progressed substantially in the seven years between the last two SMP Specialists' Meetings in spring 1977 and fall 1984. Moreover, it was also shown at the last meeting that encouraging three-dimensional methods are now emerging to predict unsteady airloads for transonic flutter analyses of clean wings. In order to assess the applicability of these prediction techniques for engineering-type practical aeroelastic analysis, the desirability of re-establishing a set of standard configurations for comparisons of calculated and measured dynamic aeroelastic behaviour under high subsonic to transonic flow conditions was discussed at the fall 1984 meeting of the AGARD-SMP Subcommittee on Aeroelasticity. Hence, two 2-D airfoils were chosen in an initial selection at the last SMP meeting in spring 1986 as transonic aeroelastic standard configurations. Assuming further progress in the development of transonic flutter prediction methods it is hoped that the selection of these standard configurations will be completed by including a more straightforward 3-D wing with supercritical profile, a low aspect ratio fighter-type swept wing, a wing with controls, etc. The cooperative AGARD program and activities based on and dictated by these standard aeroelastic configurations, then, should culminate in another symposium on "Transonic Unsteady Aerodynamics and Its Aeroelastic Applications" to be held in 1990—1991.

In order to discuss strategies for promoting engineering-level transonic aeroelastic prediction techniques and to establish tops for further research work, a Workshop entitled

"Future Research on Transonic Unsteady Aerodynamics
and Its Aeroelastic Applications"

has been held under the auspices of the SMP-Subcommittee on Aeroelasticity at the fall 1986 AGARD-SMP Meeting in Athens. Two of the keynote papers presented at this Workshop are published in this Report.

<div align="center">

H.Försching
Chairman, Subcommittee on
Aeroelasticity

</div>

ABSTRACT

This Workshop focused on strategies for promoting and developing engineering-level transonic flutter prediction techniques.

The technology of transonic aerodynamics is currently undergoing rapid development. Significant progress is being made to solve the inherently nonlinear equations describing unsteady motions of wings in transonic flow, while the availability of reliable and efficient computational methods will greatly enhance the ability to predict the aeroelastic behaviour of modern aircraft operating under transonic flow conditions.

AGARD-SMP has previously coordinated unsteady aerodynamic research carried out on a number of "standard" wind tunnel model configurations and published the results. The proposals contained in the Evaluation Report (W.J.Mykytow) on the Fall 1984 Structures and Materials Panel Specialists' Meeting on "Transonic Unsteady Aerodynamics", together with an expanded range of aeroelastic configurations, formed the guidelines which this Workshop followed.

Two of the keynote papers presented at this Workshop are published in this Report.

* * *

Cet Atelier a concentré ses efforts sur les stratégies visant à promouvoir et à développer des techniques de prévision du flottement en vol transsonique au niveau de l'ingénierie.

La technologie de l'aérodynamique transsonique fait actuellement l'objet d'un développement rapide. Des progrès significatifs sont réalisés dans la résolution des équations fondamentalement nonlinéaires décrivant les mouvements instationnaires des ailes dans le flux transsonique, alors que la disponibilité de méthodes de calcul fiables et efficaces augmenteront considérablement la possibilité de prévoir le comportement aéroélastique des avions modernes volant dans des conditions de flux transsonique.

Le Groupe chargé des Structures et des Matériaux de l'AGARD a précédemment coordonné les travaux de recherche sur l'aérodynamique instationnaire effectués sur un certain nombre de configurations de maquettes de soufflerie "standards" et en a publié les résultats. Les propositions contenues dans le rapport d'évaluation (W.J.Mykytow) établi à l'issue de la réunion, à l'automne 1984, des spécialistes du Groupe chargé de l'étude des Structures et des Matériaux, sur "l'Aérodynamique Transsonique Instationnaire", ainsi qu'une vaste gamme de configurations aéroélastiques, ont été successivement examinées par l'Atelier au cours de ses travaux.

Deux des documents clefs présentés au cours de la réunion de cet Atelier sont publiés dans ce Rapport.

CONTENTS

DEVELOPMENT OF COMPUTATIONAL METHODS FOR UNSTEADY AERODYNAMICS
AT THE
NASA LANGLEY RESEARCH CENTER

E. Carson Yates, Jr.
Chief Scientist
Loads and Aeroelasticity Division

Woodrow Whitlow, Jr.
Group Leader, Methods Development Group
Unsteady Aerodynamics Branch
Loads and Aeroelasticity Division
NASA Langley Research Center
Hampton, Virginia 23665-5225
U. S. A.

SUMMARY

The current scope, recent progress, and plans for research and development of
computational methods for unsteady aerodynamics at the NASA Langley Research Center are
reviewed. Both integral-equation and finite-difference methods for inviscid and
viscous flows are discussed. Although the great bulk of the effort has focused on
finite-difference solution of the transonic small-perturbation equation, the
integral-equation program is given primary emphasis here because it is less well known.

INTRODUCTION

Progress in the development of computational methods for steady and unsteady
aerodynamics has perennially paced advancements in aeroelastic analysis and design
capabilities. These capabilities, in turn, are of growing importance in the analysis
and design of high-performance aircraft as well as other types of flight vehicles.
Consequently, considerable effort has been directed toward the development of
appropriate unsteady-aerodynamic methodology in the NATO countries and elsewhere. This
paper reviews the contributions to those efforts at the NASA Langley Research Center.
Specifically, the current scope, recent progress, and plans for research and
development of both integral-equation and finite-difference methods for inviscid and
viscous flows are discussed, and example applications are shown. Although the great
bulk of the effort in recent years has focused on finite-difference solution of the
transonic small-perturbation equation, the integral-equation program is given primary
emphasis here because it is less well known.

INTEGRAL-EQUATION METHODS

The Langley integral-equations program is directed toward general, accurate, efficient,
and unified treatment of flows around vehicles having arbitrary shapes, motions, and
deformations (including control motions) at subsonic, transonic, and supersonic speeds
up to high angles of attack. Special attention is given to real-world design and
operating conditions (e.g., Mach number, angle of attack, maneuver) as well as to
efficient computation for both design and analysis applications. As will be brought
out in the subsequent discussion, the integral-equation approach is well suited for
these purposes because flow complexities such as viscous effects or transonic flow need
to be addressed only in the flow regions where they actually occur, and there is no
requirement for patching and matching flow domains or regional solutions. Moreover,
for design applications repetitive and nonrepetitive portions of the computations are
readily separable, and the required sensitivities of aerodynamic parameters to
variations in aircraft geometry can be readily calculated. Although the
integral-equations research program has been given only limited and intermittent
support for the last several years, it has nevertheless produced some significant
results.

Following a long-range plan established a number of years ago (fig. 1), initial efforts
addressed the development of surface-panel methods for subsonic (refs. 1 to 5) and
supersonic (refs. 1, 2, 6, 7) linearized potential flow. Current activities include
nonlinear methods implementing the full-potential equation for high-subsonic/transonic/
low-supersonic speeds (ref. 8). Although the initial high-subsonic/transonic
proof-of-concept codes (refs. 9 to 11) implemented the small-perturbation potential
equation, there is no particular benefit in refining codes for small-perturbation
conditions or two-dimensional flow as stepping-stones toward more realistic
conditions. Consequently, these items have been deleted from the original plan (fig.
1). Some computations for two-dimensional flow are made in order to conserve computer
resources, however.

Another change from the original plan (fig. 1) shows that the Euler equations are not addressed explicitly in this program. Modification of the full-potential equation to account for entropy changes across shock waves (e.g., as in ref. 12) should greatly expand the usefulness of potential-flow solutions well into the range of flow conditions that would otherwise require Euler solutions. Consequently, for present purposes we go directly from the modified full-potential method to the Navier-Stokes equations which are being addressed by use of the classical Helmholtz scalar/vector-potential decomposition (refs. 13 to 15). Euler solutions may, of course, be obtained from Navier-Stokes methods with zero viscosity. We are specifically concerned with several types of viscous influences: Thin wakes separating from lifting-surface edges are well represented by inviscid-flow singularities (vortex sheets). Other viscous influences require solution of Navier-Stokes equations or equivalent. These influences include boundary-layer effects, especially on deflected and/or deflecting control surfaces, shock/boundary-layer interaction, and large areas of flow separation in general. Specifics of these problem areas are addressed in the subsequent sections of this paper.

The time-dependent full-potential partial differential equation

$$\nabla^2 \phi - \frac{1}{a_\infty^2} \left(\frac{\partial}{\partial t} + U_\infty \frac{\partial}{\partial x} \right)^2 \varphi = F \tag{1}$$

is the governing equation for most of the work described herein. Application of the generalized Green's-function method to this equation yields an equivalent integral equation for the velocity potential ϕ at any point P in the flow or on the surface of a body in the flow at any time t (ref. 1).

$$\phi(P,t) = \underbrace{\int \int \int \int GF \, dV_1 \, dt_1}_{\text{nonlinear terms}}$$

$$\underbrace{+ \int \int \int \left[\nabla_1 S \cdot (G\nabla_1\phi - \phi\nabla_1 G) - \frac{1}{a_\infty^2} \frac{dS}{dt_1} \left(G \frac{\partial\phi}{\partial t_1} - \phi \frac{\partial G}{\partial t_1} \right) \right] |\square S|^{-1} \, dS \, dt_1}_{\text{linear terms}} \tag{2}$$

where ϕ is the perturbation velocity potential, G is the Green's function, F represents all the nonlinear terms, a_∞ is the freestream speed of sound, U_∞ is the freestream speed, x is the coordinate in the freestream direction, $S(x,y,z,t) = 0$ defines the body surface, and

$$|\square S| = \sqrt{S_x^2 + S_y^2 + S_z^2 + S_t^2}$$

The exact boundary condition on the body surface is

$$\frac{DS}{Dt} = 0 \tag{3}$$

The time integration with respect to t_1 in equation (2) is made trivial by choice of a subsonic or supersonic source pulse as the Green's function.

An important point here is that only the nonlinear terms need to be integrated over a fluid volume. The linear terms are integrated only over the surface of the body and its wake. Note also that the Green's function is a function of freestream Mach number, not local Mach number. Equations (2) and (3) have been formulated and computationally implemented in a moving frame of reference so that they are applicable to problems such as helicopter rotors and maneuvering aircraft as well as aircraft in uniform motion (refs. 16 to 19).

Linearized Theory

If perturbations from freestream velocity are small, and Mach number is not near one nor too high in the supersonic range, the non-linear terms are negligible, and the volume integral can be ignored. The remaining surface integral of the linear terms is discretized by surface paneling (ref. 2) (e.g., arbitrary twisted quadrilateral panels as in refs. 3 and 4). The unsteady-flow solution can then be obtained directly by integration in time domain, or a time solution by Laplace transform (refs. 2 to 4) converts to a complex-frequency domain formulation which is generally more efficient for use in solving linear aeroelastic problems.

The velocity potential on the paneled surface is then found in terms of the normalwash distribution which, in general, is known from the input shape, orientation, motion, and deformation.

$$[Y_{jh}] \{ \tilde{\phi}_h \} = [Z_{jh}] \{ \tilde{\psi}_h \} \tag{4}$$

where $\tilde{\phi}_h$ is the Laplace transform of the perturbation velocity potential, and $\tilde{\psi}_h$ is the Laplace transform of the normalwash

$$Y_{jh} = \delta_{jh} - (C_{jh} + sD_{jh}) e^{-s\theta_{jh}} - \sum_h (F_{jn} + sG_{jn}) S_{nh} e^{-s(\theta_{jn} + \pi_n)} \tag{5}$$

$$Z_{jh} = B_{jh} e^{-s\theta_{jh}} \tag{6}$$

δ_{jh} is Kronecker delta, s is the Laplace transform variable (complex frequency), $B_{jh}, C_{jh}, D_{jh}, F_{jn}, G_{jn}$ are integrals over surface panels, Θ_{jh}, π_{jn} are lag functions, and $S_{nh} = \pm 1$ for panels adjacent to a trailing edge on upper or lower surface of the body and is zero otherwise. Surface pressures are obtained from the potential by use of Bernoulli's equation.

Several features of equations (4) to (6) are significant. First, the elements of the Y and Z influence matrices are independent of the normalwash and hence independent of the mode of motion or deflection. Moreover, these matrix elements are simple functions of the complex frequency s so that the cost of changing frequency or calculating for multiple frequencies is small. The influence integrals B, C, and D represent integrals of source, doublet, and "ratelet" distributions over each body-surface panel, and integrals F and G are the corresponding doublet and "ratelet" integrals for wake panels. For a given paneling geometry, all of these integrals are functions only of Mach number. If a problem (e.g., dynamic response or flutter) involves multiple modes of normalwash, the normalwash vector in the equation becomes a matrix of modal columns, and the potential distributions for all the modes can be found in a single solution. Similarly, solutions for additional modes or revised modes (as in a structural-design optimization problem) can be obtained without recalculating the Y and Z matrices. For use in design processes, this formulation also appears to provide a general and very efficient means for evaluating sensitivities, i.e., changes in aerodynamic properties caused by changes in external shape. Demonstration calculations have been initiated.

The generality and versatility of this approach is indicated by its use by Rockwell International for flutter analysis of the space shuttle (fig.2) in the mid 1970's. Nearly 800 panels were used on the orbiter, and up to 60 modes of motion were used in both symmetric and antisymmetric flutter analyses. Subsequently, the external tank and solid rocket boosters were added, and the calculations were repeated for the entire launch configuration.

For development purposes equations (4) to (6) have been implemented in a prototype code called SOUSSA P1.1 (Steady, Oscillatory, and Unsteady Subsonic and Supersonic Aerodynamics - Version 1.1) (refs. 3 and 4) which is applicable to vehicles having arbitrary shapes, motions, and deformations in subsonic flow only. The P1.1 code employs zeroth-order (constant-potential) panels along with the data base and data-handling utilities of the SPAR finite-element structural-analysis program. These were incorporated because SOUSSA P1.1 originally was intended for the calculation of steady-state structural loads and unsteady aerodynamics for flutter and gust-response calculation in multidisciplinary structural-optimization computations employing the SPAR structural analysis. The SPAR components, however, are unnecessary for stand-alone use. More efficient data handling methods for stand-alone operation are available.

Subsequent to the completion of SOUSSA P1.1 several significant improvements have been incorporated, and others have been defined (ref. 5). Among the latter are implementation of higher-order panels, elimination of the SPAR components, transposition and revision of the solution algorithm to substantially reduce input/output operations, and improved implementation of the trailing-edge (Kutta) flow condition.

Some program improvements already incorporated in the SOUSSA code include the development of an "out-of-core" solver to permit the use of paneling schemes that lead to coefficient matrices too large to fit in the memory of modest-size computers; the replacement of the paneled wake by an analytical wake (reducing the cost of a typical run by about one-half) but retaining an option to use paneled wakes if needed (e.g., when there is another lifting surface in the wake); and replacing the rectangular integration of pressures by a Gaussian quadrature scheme to improve the accuracy of the calculated generalized aerodynamic forces. These improvements are incorporated in a replacement for the SOUSSA code (called UTSA) which is under development at a low level of effort.

Figure 3 (reproduced from ref. 5) compares a chordwise distribution of pressure coefficient C_p calculated by the SOUSSA surface-panel method with pressures measured on a clipped delta wing oscillating in pitch (ref. 20). The wing had a six-percent-thick circular-arc airfoil. The agreement is good and is representative of results obtained with this code. Figure 4 compares calculated and measured steady upper-surface pressures at two chordwise locations x on an outboard station (y=0.85) on the same clipped delta wing. Two points are to be made: First, in the range of angle of attack α (-2 deg to +2 deg) where pressure varies linearly, the agreement is excellent. Second, for this sharp-edge wing, the influence of the leading-edge vortex is substantial and begins at a low angle of attack. The latter behavior emphasizes the importance of our treatment of vortex-type flow separation to be discussed below. A phenomenological description of the relation between the vortex development and the pressure variation shown is given in ref. 21 (from which figure 4 was taken) and in Appendix A of ref. 20.

In addition to the subsonic capability of the SOUSSA program, a supersonic proof-of-concept surface-panel code has been written to implement linear-theory

algorithms developed in refs. 6 and 7. The code employs first-order panels and, like SOUSSA, is applicable to vehicles having arbitrary shapes, motions, and deformations. Validation and application of the code have begun.

The only significant difference between subsonic and supersonic formulations is in the expressions for the influence integrals B,C,D, F,G in equations (5) and (6) (see, e.g., ref.2). Other portions of the computations, such as paneling geometry and solution alorithms are common to both. Consequently, it is possible that the computational capability for supersonic flow derived from this proof-of-concept code will subsequently be incorporated into the subsonic code UTSA.

The status and near-term plans for linear-theory surface-panel methods, which are applicable to vehicles having arbitrary shapes, motions, and deformations, may be summarized as follows: As planned the SOUSSA program will be superseded by an improved program UTSA which incorporates first-order panels as well as other improvements indicated by earier work with SOUSSA. Ultimately, the code may include both subsonic and supersonic capabilities. Frequency-domain computations are most efficient for implementing linear theory, but a time-domain version is also retained for evaluation of the surface integral in the nonlinear methods described next. Specific activities include configuring the UTSA code for efficient use in interdisciplinary design processes, incorporating special elements to improve accuracy and efficiency near normalwash discontinuities (e.g., at control surfaces), completing the initial demonstration of the efficient computation of sensitivities of aerodynamic pressures and loads to variations in planform, and general check out and validation.

Nonlinear Theory

When the flow approaches transonic conditions and/or flow perturbations (e.g., angle of attack) become large, the nonlinear terms represented by F in equation (2) are no longer negligible, and the volume integral must be evaluated in combination with the surface-panel evaluation of the linear terms (refs. 9 to 11). For nonlinear problems it is important to note (1) that the Green's function depends on freestream Mach number, not local Mach number, and (2) that the integrand of the volume integral diminishes rapidly in magnitude with increasing distance from the body and its wake.

For application to nonlinear problems the integral-equation method has several features which make it particularly attractive for general, efficient computational implementation: (1) Evaluation of an integral is required rather than the numerical solution of a partial differential equation, which is a more sensitive process. (2) The volume integral need be treated only in the limited region of flow in which nonlinear terms are of significant magnitude rather than over an entire computational domain. In fact, as the integration proceeds away from the body, it is terminated when the integrand falls below a preselected threshhold value. (3) Required accuracy can be attained with relatively few computational grid points in the fluid (computational domain of the volume integral). (4) The code is numerically stable even when moderate-to-large time steps are employed. (5) Correct far-field boundary conditions are automatically imposed. This condition is particularly important for unsteady flow. Linear-theory behavior in the far field is inherent in the integral-equation solution. (6) When viscous flows are treated by the scalar/vector-potential decomposition (to be discussed below), interfacing (patching and matching) of regional solutions (e.g., inner viscous solution and outer inviscid solution) is not required. (7) Even for solution of the full-potential equation, there is no requirement for generating, imbedding, or interpolating surface-fitted computational grids.

In this section small-perturbation transonic attached flow will be considered first followed by large-perturbation subsonic and transonic flow conditions involving vortex-type flow separation in the form of thin wakes emanating from lifting-surface edges and finally flow conditions involving significant viscous effects which require solution of Navier-Stokes equations for attached or separated flow for which the scalar/vector-potential method is employed.

Small-Perturbation Transonic Flow: For proof-of-concept demonstration of transonic capability, only the small-perturbation terms were retained in the volume integral of equation (2), and the resulting time-domain computer code (ref. 11) was called SUSAN (Steady and Unsteady Subsonic Aerodynamics-Nonlinear). Figure 5 shows chordwise pressure distribution near the root of a rectangular wing as calculated by the SUSAN code and by a transonic small-perturbation finite-difference code. The shock is captured, and the agreement is quite good even though only a few elements were used to evaluate the volume integral, and the domain of integration extended only one chord length from the wing perimeter. Good agreement with measured pressures (from ref. 22) is shown in figure 6 for a sharp-edge wing under conditions involving supercritical flow over much of the chord.

Evolution of the lifting pressure ΔC_p on a wing oscillating slowly in pitch about the leading edge is shown in figure 7 at three times during a cycle of motion. Although only ten computational elements along the wing chord were used to evaluate the volume integral of the nonlinear terms, the build-up of lift and the appearance of a shockwave are clearly indicated. In this particular figure, the symbols shown are used only to distinguish the curves and do not indicate computational points.

The formulation described here and its implementation in the SUSAN code demonstrated the merits of the integral-equation method for transonic flow. However, no further development of the small-perturbation approximation is planned.

Subsonic/Transonic Flow with Vortex Separation: All of the preceding involved calculation of the velocity potential. For solving nonlinear problems, however, there are advantages in calculating velocities directly, especially when large velocity variations occur, when shocks are present, when thin-wake (vortex-like) flow separation from wing leading or side edges occurs (fig. 8), or even when trailing-edge wake deformations are significant. Taking the gradient of the integral equation for the potential (equation (2)) or alternatively applying the Green's-function method to the full-potential equation in the form (for steady state)

$$\nabla^2 \phi = \frac{-1}{\rho} \nabla\rho \cdot \nabla\phi \equiv Q \qquad (7)$$

gives (ref. 8)

$$\vec{V}(x,y,z) = \vec{E}_\infty + \frac{1}{4\pi} \iint_{BODY} \frac{\vec{\omega} \times R}{R^3} \, dS + \frac{1}{4\pi} \iint_{WAKE} \frac{\vec{\omega} \times R}{R^3} \, dS \qquad (8)$$

$$+ \frac{1}{4\pi} \iiint_{VOL.} \frac{Q}{R^2} \vec{E}_R dV$$

where ρ is the fluid density, $\vec{\omega}$ is the vorticity vector, R is the vector from "sending" point to "receiving" point, $\vec{E}_R$ is a unit vector in the R direction, and $\vec{E}_\infty$ is a unit vector in freestream direction.

Equation (8) is an expression for the velocity field $\vec{V}$ as the sum of four components: (1) freestream, (2) a surface integral which gives the velocity induced by the flow singularities representing the solid body, (3) a surface integral which gives the velocity induced by the vorticity representing the thin wake, and (4) a volume integral representing the compressibility terms (right-hand side of equation (7)). The integrand of this volume integral decreases more rapidly than the square of the distance from the body or vortex surface, so the domain of integration can be relatively small. The integrands in the three integrals are not independent, and solution is by iteration to satisfy the boundary conditions on the body and to deform the free vortex sheets into a force-free shape (ref. 8). Note that the form of the integrand shown in the body integral indicates the use of a vorticity distribution to represent a thin wing in some proof-of-concept calculations. One of the major generalizations of this method, to be initiated, consists of replacing this body integral with the UTSA surface-panel formulation so that transonic flow over bodies of arbitary shape, including vortex-type separation, can be calculated. Other planned improvements include (1) replacing the vortex-lattice model used in the wake integral for proof-of-concept calculations with the hybrid-vortex formulation (refs. 23 and 24) in which second-order distributed-vorticity panels are used to compute near-field influence, reducing to zeroth-order (discrete-vorticity) elements for far-field influence, (2) shifting the linear compressibility term $M^2\phi_{xx}$ from volume integral to surface integral by solving

$$\nabla^2 \phi - M^2 \phi_{xx} = Q - M^2 \phi_{xx} \equiv Q_{nonlin} \qquad (9)$$

instead of equation (7), thereby significantly reducing the region over which the volume integral needs to be evaluated, (3) replacing constant source strength with linearly varying source strength in the volume elements and introduing a threshold cutoff value for the integrand of the volume integral to terminate integration when the integrand diminishes to negligible magnitude, (4) accelerating convergence of the solution by possible use of shock fitting (ref. 8), (5) accounting for entropy changes across shockwaves (see, e.g., ref. 12). Code development for unsteady flow is in progress. Research on suitable configuration of these codes for efficient use in computer-aided interdisciplinary design will be a continuing activity.

Completion of the improvements listed above should provide a powerful tool for calculating transonic and/or free-vortex flows around arbitrary aircraft configurations with sharp leading edges or with specified separation line locations. Establishing the separation line on a vibrating wing, however, is a tough viscous-flow problem, but may be amenable to treatment by the scalar-vector potential method to be discusssed below. The importance of expediting this activity should be underscored. The ability to calculate accurately the complicated transonic vortical flows around highly swept wings and complete aircraft at high angles of attack is a key problem for the future development of highly maneuverable fighter aircraft and is already needed to improve the assessment and understanding of steady and transient flight loads and flutter problems of current combat aircraft. It should be especially noted that vortex-type flow separations produce typically detrimental effects on structural loads and flutter.

Figure 9 shows the calculated velocity field and shape of the free-vortex surface in a crossflow plane slightly downstream of the trailing edge of a delta wing with vortex sheets representing thin wakes emanating from leading and trailing edges as in figure 8. The volume integral (equation (8)) has not been included for this incompressible-flow calculation. The results compare quite favorably with the low-Mach-number

experiments of Hummel (ref. 25) even though relatively few vortex elements were used in this exploratory calculation. The leading-edge vortex core is clearly defined as is the incipient deformation of the trailing-edge vortex sheet into a trailing-edge core with rotation opposite to that of the leading-edge core. The corresponding spanwise distributions of lifting pressure ΔC_p are shown in figure 10 for crossflow planes at 0.7 and 0.9 of the root chord aft of the wing apex. Agreement with measured values is very good.

Inclusion of the volume integral (equation (8)) permits calculation of transonic flow. Figure 11 shows the spanwise distribution of upper-surface pressure C_{pu} and the flow field, including a captured shock, in a crossflow plane at 0.8 of the root chord aft of the apex of a delta wing (ref. 8). In this exploratory calculation the vortex sheet was not allowed to roll up enough to exert its full inductive effect on the wing surface before the vorticity was transferred into the vortex core. If an additional quarter turn of rollup were allowed, the pressure peak would be slightly higher and a little farther outboard, resulting in even better agreement with experiment. In contrast, the pressure peak from the Euler solution is considerably weaker and farther outboard than the experimental peak because of spatial and numerical diffusion in the Euler calculation.

Structural design loads do not occur at small-perturbation conditions but at limit load-factor conditions such as high angle of attack. Aeroelastic deformations are important. Wind-tunnel results may be of questionable accuracy because of large wall effects. The important influence of large perturbation conditions and free-vortex flows on structural design loads is typically detrimental, as is illustrated by the calculations shown in figure 12 (from ref. 26). Even if the linear and nonlinear spanwise load distributions shown were compared on the basis of same total normal force (same area under the curves), it is evident that the effect of the wing-tip vortex is to shift the load outboard and hence increase wing bending movements.

Linearized aerodynamic theory indicates that there should be no effect of angle of attack on flutter dynamic pressure. However, a detrimental effect typically does occur with increasing angle of attack (see, e.g., refs. 27 and 28). If adequate flutter margins are to be maintained when angle of attack is not near zero, the degradation must be predictable. Wind-tunnel testing of stiffness-scaled flutter models is not the answer because they are typically too weak to sustain more than very small static loads. Figure 13 shows experimental variation of flutter dynamic pressure with angle of attack for a stiff wing that was spring supported (ref. 29). The initial decline in flutter dynamic pressure between 0 and 7 deg is attributed to the effect of the tip vortex. Confirming calculations by methods just described are in early stages. The drastic decline beyond 7 deg is probably caused by flow separation progressing forward from the trailing edge. Prediction of that behavior will require solutions of Navier-Stokes equations as discussed below.

Summarizing the status of integral-equation methods for vortex-type (thin wake) flow separation: The hybrid-vortex method for low-Mach-number steady flow (refs. 23 and 24) is complete. Computations based on equation (8) for steady transonic flow with vortex-type separation and shockwaves have been demonstrated (ref. 8), and the corresponding unsteady code development is in progress. Major generalizations and improvements in efficiency are underway. Further developments for transonic flow, with or without vortex-type flow separation, will be based on equation (8).

Scalar/Vector-Potential Method: When viscous influences (other than thin wakes from lifting-surface edges) are important -- for example, boundary-layer effects on control-surface forces, shock/boundary-layer interaction, or flow separation from surfaces (fig. 1) -- solution of Navier-Stokes equations in some form is required. The approach taken here is a scalar/vector-potential (SVP) decomposition of the velocity field by use of the classical Helmholtz representation of a vector field as the sum of an irrotational part and a solenoidal part (refs. 13 to 15). Thus

$$\bar{v} = \text{grad } \phi + \text{curl } \bar{A} \tag{10}$$

where ϕ is again the scalar potential which is evaluated by the methods already described herein, and the vector potential $\bar{A}$ is related to the vorticity $\bar{\omega}$ by

$$\nabla^2 \bar{A} = -\bar{\omega} = -\text{curl } \bar{v} \tag{11}$$

The vorticity, in turn, is governed by the vorticity-dynamics equation

$$\frac{D}{Dt}\left(\frac{\bar{\omega}}{\rho}\right) - \frac{\bar{\omega}}{\rho} \cdot \text{grad } \bar{v} = \frac{1}{\rho} \text{curl } \bar{A}$$

$$= \frac{1}{\rho} \text{grad } T \times \text{grad } S + \frac{1}{\rho} \text{curl } \frac{1}{\rho} \text{div } (T + pI) \tag{12}$$

which is obtained by taking the curl of Navier-Stokes equation for general, three-dimensional, unsteady, compressible, viscous, heat-conducting flow (ref. 13) to which the present formulation is fully equivalent. In equation (12), T is temperature, S is entropy, and $\bar{T}$ is stress tensor.

The formulation in equations (10) to (12) appears to be a computationally attractive alternative to direct solution of the Navier-Stokes equations in primitive variables. Methods of this type have been used for a long time for viscous incompressible flow, but they have not proved to be readily generalizable to compressible flow. The present formulation is quite general and is directly applicable to compressible flow. Since the outer region of the flow about an aircraft is essentially irrotational, an integral-equation implementation appears to be an especially attractive method of solution. The initial proof-of-concept code for two-dimensional incompressible flow has been used to calculate boundary layers on a flat plate (fig. 14), flow over an airfoil, and separated flow around a rectangle (fig. 15) -- all with good results (refs. 14 and 15). In particular, the calculation of flow around a rectangle (fig. 15) demonstrates the ability to calculate flows involving large regions of separation. The resulting velocity field shown in the figure illustrates that flow separation is predicted very satisfactorily even though separation was not imposed by any artificial means within the algorithm. These results are in excellent agreement with the finite-difference results of ref. 31. Application to a circulation-control airfoil is being initiated. For applications to turbulent flows this method, of course, requires a good turbulence model just as any other method does. In addition to its computational use, the SVP formulation has also generated considerable insight into the relations between surface boundary conditions, viscosity, vorticity and its diffusion (refs. 14 and 15).

Current activities are extending the proof-of-concept code to three dimensions and to compressible flow. The types of applications planned include viscous flow over lifting surfaces with and without control-surface deflection, lifting surfaces with flow separation from edges in compressible flow, and lifting surfaces with separated flow following a step change in angle of attack.

Summary of Integral-Equation Activities

The activities described here and the computational capabilities summarized in table I indicate that completion of this work will provide efficient and unified treatment of flow over vehicles having arbitrary shapes, motions, and deformations at subsonic, transonic, and supersonic speeds up to high angles of attack. Moreover, the computational forms of the equations and the computational capabilities that are emerging appear to be well suited for repetitive use in design applications as well as for stand-alone use. As pointed out previously, the UTSA surface-panel program for attached flow may contain both subsonic and supersonic modules in a single program. Flow complexities, such as transonic nonlinearities, thin wakes, or viscous influences, are addressed only if and where they occur. Thus, if the volume-integral module is included with UTSA, the program implements the full-potential equation for transonic nonlinear attached flow. With modification for shock-generated entropy change, the program can apply also to flows with shocks of finite strength, including supersonic Mach numbers above the linear range, as long as shock-generated vorticity is of minor importance. If the hybrid-vortex module representing the free vortex sheets is also included, the code treats transonic flow with vortex-type separation. Finally, combination of the vector potential with these scalar-potential methods (SVP formulation) permits the formal equivalent of Navier-Stokes solutions for high angles of attack where flow separation from surfaces may occur (for example, on advanced fighter aircraft in combat maneuvers and in highly transient conditions) and also even for low angles of attack when control-surface deflections or deflection rates are large enough or shock waves are strong enough to cause significant boundary-layer thickening or separation. The latter conditions are particularly important for generating control forces and for design of active control systems.

FINITE-DIFFERENCE METHODS

The goal of this activity is to develop finite difference methods that can be used for aeroelastic analysis of complete aircraft. At the Langley Research Center, efforts based on transonic small perturbation (TSP) potential theory, full potential theory, and the Euler/Navier-Stokes equations are underway.

Transonic Small-Perturbation Equation

At the TSP level, development has progressed on two fronts--(1) extending the capability of the XTRAN3S code (ref. 32) through extensive modification and (2) developing a new program (ref. 33). Fig. 16 shows a sample wing/fuselage calculation made possible by modifying XTRAN3S (ref. 34). The wing has an RAE 101 airfoil section, 37 deg leading edge sweep angle, aspect ratio (AR) of 6, and taper ratio of one-third. The fuselage is a sting-mounted, axisymmetric body of revolution with fineness ratio (length/maximum diameter) of 7.66. Calculations were made for a flexible wing at free stream Mach number (M) of 0.91 and mean angle of attack (α) of 1 deg. Fig. 16 (a) shows the wing tip deflection as a function of time, and fig. 16 (b) shows the gridding used to represent the wing/fuselage. Figs. 16 (c) and 16 (d) show the instantaneous Mach number contours at the maximum and minimum tip deflections, respectively. The wing motion is the first bending mode at a reduced frequency (k) of 0.25. The contours

near the leading and trailing edges indicate local Mach numbers less than 0.85, and over the wing chord and fuselage, the contours indicate Mach numbers greater than 0.95.

A new TSP code, CAP-TSD (Computational Aeroelasticity Program-Transonic Small Disturbance) (ref. 33) has been developed at Langley. It solves the three-dimensional (3-D) TSP equation using an approximate factorization (AF) algorithm. The code is significantly more efficient than methods that use an alternating-direction-implicit (ADI) solution algorithm and can be used for aeroelastic analysis of complete aircraft. Fig. 17 shows comparisons of CAP-TSD (AF) and XTRAN3S (ADI) calculations with experimental data for a rigid F-5 wing pitching about zero mean angle at k = 0.137 (ref. 35). Pressures are shown at the 51 percent span station ($\bar{\eta}$). Upper surface pressures are shown in fig. 17 (a), and lower surface pressures are shown in fig. 17 (b). Both sets of calculations show good agreement with the measured data and are nearly identical to each other. The primary difference is that the AF solution requires only ten percent of the computer resources used in the ADI calculation. CAP-TSD has been used to compute steady flow past a wing/fuselage/tail model that was tested at DFVLR. In the test, M = 0.2, α = 0.15 deg. The wing is rectangular with RAE 101 airfoil sections (9 percent thickness ratio) and a full-span aspect ratio of 6. The horizontal tail is rectangular with RAE 101 airfoil sections (12 percent thicknessratio) and full-span aspect ratio of 3. The fuselage is an axisymmetric body of revolution with fineness ratio of 9.75. The mathematical representation of the model is shown in fig. 18 (a). Comparisons of computed and measured pressures on the wing and tail are shown in fig. 18 (b). Fig. 18 (c) shows comparisons of computed and measured pressures on the fuselage. In all cases, the computations and experiments are in good agreement.

Potential flow theory has been shown to give highly erroneous and even multivalued results when shock waves are in the flow field (refs. 36, 37). This is because shock-generated entropy is not modeled in potential flow formulations. A method for modeling nonisentropic effects in 2-D TSP theory was developed by Fuglsang and Williams (ref. 12) and extended to three dimensions by Gibbons et al. (ref. 38). The nonisentropic formulation was implemented by modifying the streamwise flux in the TSP equation to account for entropy jumps across shock waves. This alleviates the phenomena of multiple solutions and highly inaccurate loading predicted by isentropic potential methods. Fig. 19 shows an example of calculated lift as a function of angle of attack for isentropic and nonisentropic formulations. An Euler calculation is included at one deg angle of attack. Without the nonisentropic corrections, the calculated lift is too large. When the corrections are included, the calculated lift is less and agrees with the Euler calculation at the point where such data is available.

Full-Potential Equation

A method for modeling shock-generated entropy in the unsteady full-potential (FP) formulation has been developed at Langley (ref. 39). The method is an extension of the steady-flow method of Hafez and Lovell (ref. 40). Fig. 20 shows the instantaneous pressures on an NACA 0012 airfoil oscillating in pitch about its quarter chord. In this case, M = 0.755, $\alpha(t)$ = (0.016 + 2.51sin(kt)) deg, and k (based on semichord) = 0.0814. Fig. 20 (a) shows a comparison of the isentropic full-potential method, a TSP method (denoted by "TSD" on the figure) (ref. 41), and experimental data (ref. 42). Fig. 20 (b) shows isentropic and nonisentropic full potential methods, along with the measured data. When entropy corrections are used, more accurate modeling of the shock is obtained, and agreement with the measured data is improved.

Currently, efforts are underway to extend the full potential method to three dimensions. The proposed method will have the capability to do aeroelastic analysis for flows in the subsonic, transonic, and supersonic speed ranges.

Euler/Navier-Stokes Equations

Research is being conducted to develop methods for obtaining time-accurate unsteady solutions of the Euler/Navier-Stokes equations. These methods are used to solve the Navier-Stokes equations, with solutions of the Euler equations obtained by turning off the viscous terms. The existing codes are used to march in time to steady state and currently are being modified to be made time-accurate. An effort is underway to correlate Navier-Stokes calculations with pressure data measured in the Langley Research Center 0.3-meter Transonic Cryogenic Tunnel. Unsteady transonic pressures were measured on a 14-percent-thick supercritical airfoil at cryogenic temperatures for M between 0.65 and 0.74 and at Reynolds numbers based on airfoil chord (Rc) between 6 million and 35 million (ref. 43). The model is shown in fig. 21 (a). The open symbols in fig. 21 (b) show test conditions where the effects of frequency on the unsteady pressures were examined, and the solid symbols show where the effects of frequency and amplitude were studied. Steady pressure distributions at Rc = 6 million (open symbols) and at Rc = 30 million (solid symbols) are shown in fig. 21 (c). The results of this study may be used to determine when various forms of the Navier-Stokes equations can be used (e. g., thin-layer or the full equations) and may be used to evaluate methods that couple viscous flow models with inviscid methods.

An implicit upwind code that can be used to calculate massively separated 2-D flows (ref. 44) is available for use in the correlation study. It uses van Leer flux-vector splitting and is first-order accurate in time and second-order accurate in space. The

method can be used for time marching to steady-state solutions, but it is not time-accurate and cannot model unsteady flow. An example of the capability of this code is shown in fig. 22. Even though the code is not time accurate, the example shows the variation in loads that can occur when marching to steady state. It shows computation of laminar flow about a 12-percent-thick Joukowski airfoil at 53 deg angle of attack at minimum lift (fig. 22 (a)), increasing lift (fig. 22 (b)), and maximum lift (fig. 22 (d)) for a Strouhal number of 0.166. The time history of the lift is shown in fig. 22 (c). At minimum lift, a strong counterclockwise vortex has just been shed from the trailing edge. There is a weak region of clockwise vorticity one-half chord behind the airfoil and a strong region of clockwise vorticity, which persists throughout the entire cycle, at the leading edge. The flow near the upper surface is broken into several cells of vorticity. As the lift increases, the trailing edge vortex breaks away and weakens as the region of clockwise vorticity behind the airfoil increases in strength. The vorticity near the upper surface becomes predominantly counterclockwise. Current efforts are aimed at extending this capability to time-accurate analysis of 2D unsteady flows.

A steady-flow Navier-Stokes method (ref. 45) is available for analysis of 3-D wings. The convective and pressure terms are upwind differenced, using a flux-vector splitting method. The shear stress and heat transfer terms are centrally differenced. The resulting algorithm is second-order accurate in space. An implicit, spatially factored algorithm, which is fully vectorized for the Control Data Corporation VPS 32, is used to provide efficient solutions. Efforts also are underway to extend this capability to 3D time-accurate analysis. An example of calculations made using this method is shown in fig. 23. It shows the contours of the calculated total pressures on an AR = 1 delta wing (75 deg leading-edge sweep angle) at M = 0.3 and α = 20.5 deg. Solutions were obtained by marching in time to steady state. Primary and secondary vorticies are evident on the upper surface. Close examination of the surface velocities indicates a tertiary separation outboard of the secondary vortices. This type of flow field also was observed in a related experiment (ref. 25).

Fig. 24 shows contours of measured total pressures on the same delta wing at the same flow conditions used in the previously mentioned Navier-Stokes calculations. These steady-flow data were measured in the Basic Aerodynamic Research Tunnel at Langley (ref. 46) and show good agreement with the calculated data in fig. 23.

Summary of Finite-Difference Activities

Areas of current activity in the development of finite-difference methods are shown in fig. 25. Methods based on TSP theory are being applied to configurations as complex as complete aircraft. Unsteady full-potential methods are being developed for 3-D configurations with the goal being to use such methods for aeroelastic analysis of complete aircraft. Steady, time-marching Navier-Stokes methods are available for airfoil and for isolated wings. Those methods are currently being made time-accurate.

CONCLUDING REMARKS

Some problems, progress, and plans in the development of steady and unsteady computational aerodynamics for use in aeroelastic analysis and design have been reviewed. The primary focus has been on applications to (1) vehicles having arbitrary shapes, motions, and deformations, (2) appropriate design and operating conditions, especially for transonic speeds and high angles of attack, (3) efficient computation of aerodynamics and aeroelastic behavior for both design and analysis. Current and future activities have been highlighted.

REFERENCES

1. Morino, Luigi: A General Theory of Unsteady Compressible Potential Aerodynamics. NASA CR-2464, 1974.

2. Morino, Luigi; and Chen, Lee-Tzong: Indicial Compressible Potential Aerodynamics Around Comlex Aircraft Configurations. In "Aerodynamic Analyses Requiring Advanced Computers" NASA SP-347, Part II, pp. 1067-1110, 1975.

3. Morino, Luigi: Steady, Oscillatory, and Unsteady Subsonic and Supersonic Aerodynamics - Production Version (SOUSSA P1.1) - Vol. I, Theoretical Manual. NASA CR-159130, 1980.

4. Smolka, Scott A.; Preuss, Robert D.; Tseng, Kadin; and Morino, Luigi: Steady, Oscillatory, and Unsteady Subsonic and Supersonic Aerodynamics - Production Version 1.1 (SOUSSA P1.1), Vol. II - User/Programmer Manual. NASA CR 159131, 1980.

5. Yates, E. Carson, Jr.; Cunningham, Herbert J.; Desmarais, Robert N.; Silva, Walter A.; and Drobenko, Bohdan: Subsonic Aerodynamic and Flutter Characteristics of Several Wings Calculated by the SOUSSA P1.1 Panel Method. AIAA Paper 82-0727, 1982.

6. Freedman, Marvin I.; Sipcic, Slobodan; and Tseng, Kadin: A First-Order Green's Function Approach to Supersonic Oscillatory Flow - A Mixed Analytic and Numerical Treatment. NASA CR-172207, 1984.

7. Freedman, Marvin I.; and Tseng, Kadin: A First-Order Time-Domain Green's Function Approach to Supersonic Unsteady Flow. NASA CR-172208, 1985.

8. Kandil, Osama A.; and Yates, E. Carson, Jr.: Computation of Transonic Vortex Flows Past Delta Wings - Integral Equation Approach. AIAA Journal, Vol. 24, No. 11, November 1986, pp. 1729-1736.

9. Morino, Luigi; and Tseng, Kadin: Time-Domain Green's Function Method for Three-Dimensional Nonlinear Subsonic Flows. AIAA Paper 78-1204, 1978.

10. Tseng, K. and Morino, L.: Nonlinear Green's Function Method for Unsteady Transonic Flows. In "Transonic Aerodynamics", edited by David Nixon. AIAA Series, Progress in Aeronautics and Astronautics, Vol. 81, 1982, pp. 565-603.

11. Tseng, K.: Nonlinear Green's Function Method for Transonic Potential Flow. Ph.D. Dissertation, Boston University, 1983.

12. Fuglsang, Dennis F.; and Williams, Marc H.: Non-Isentropic Unsteady Transonic Small Disturbance Theory. AIAA Paper 85-0600, 1985.

13. Morino, Luigi: Scalar/Vector Potential Formulation for Compressible Viscous Unsteady Flows. NASA CR-3921, 1985.

14. Morino, L.: Helmholtz Decomposition Revisited: Vorticity Generation and Trailing Edge Condition. Part 1: Incompressible Flows. Computational Mechanics, Vol. 1, 1986, pp. 65-90.

15. Morino, L.; Bharadvaj, B. K.; and Del Marco, S. P.: Helmholtz Decomposition and Navier-Stokes Equations. In "Proceedings of International Conference on Computational Mechanics", May 25-29, 1986, Tokyo, Japan.

16. Soohoo, P.; Noll, R. B.; Morino, L.; and Hamm, N. D.: Rotor Wake Effects on Hub/Pylon Flow. Vol. I, Theoretical Formulation . Applied Technology Laboratory, U. S. Army Research and Technology Laboratories (AVRADCOM), Fort Eustis, VA, USARTL-TR-78-1A, 1978, p. 108.

17. Morino,L.; Kaprielian, Z., Jr.; and Sipcic, S. R.: Free Wake Analysis of Helicopter Rotors. Vertica, Vol. 9, No. 2, 1985, pp. 127-140.

18. Morino, L.; and Bharadvaj, B. K.: Two Methods for Viscous and Inviscid Free-Wake Analysis of Helicopter Rotors. CCAD-TR-85-04-R, Boston University, 1985.

19. Bharadvaj, B. K.; and Morino, L.: Free-Wake Analysis of Helicopter Rotors: A Boundary Element Approach. BETECH 86, Proceedings of the 2nd Boundary Element Technology Conference, MIT, USA, pp. 291-303, Computational Mechanics Publications, 1986.

20. Hess, Robert W.; Cazier, F. W.; and Wynne, Eleanor C.: Steady and Unsteady Transonic Pressure Measurements on a Clipped-Delta Wing for Pitching and Control-Surface Oscillations. NASA TP 2594, 1986.

21. Yates, E. Carson, Jr.; and Olsen, James J.: Aerodynamic Experiments with Oscillating Lifting Surfaces - Review and Preview. AIAA Paper 80-0450. Invited Lecture given at AIAA 11th Aerodynamic Testing Conference, Colorado Springs, March 1980.

22. Knechtel, Earl D.: Experimental Investigation at Transonic Speeds of Pressure Distributions over Wedge and Circular-Arc Airfoil Sections and Evaluation of Perforated Wall Interference. NASA TN D-15, 1959.

23. Kandil, O. A.; Chu, L. C.; and Yates, E. C., Jr.: Hybrid Vortex Method for Lifting Surfaces with Free Vortex Flow. AIAA Paper 80-0070, 1980.

24. Kandil, O. A.; Chu, L.; and Turead, T.: A Nonlinear Hybrid Vortex Method for Wings at Large Angle of Attack. AIAA Journal, Vol. 22, No. 3, March 1984.

25. Hummel, D. J.: On the Vortex Formation Over a Slender Wing at Large Angles of Incidence. AGARD CP 247, 1978.

26. Kandil, Osama A.: Prediction of the Steady Aerodynamic Loads on Lifting Surfaces Having Sharp-Edge Separation. Ph.D. dissertation, Virginia Polytechnic Institute and State University, 1974.

27. Houwink, R.; Kraan, A. N.; and Zwaan, R. J.: Wind-Tunnel Study of the Flutter Characteristics of a Supercritical Wing. Journal of Aircraft, Vol. 19, No. 5, May 1982, pp. 400-405.

28. Yates, E. Carson, Jr.; Wynne, Eleanor C.; and Farmer, Moses G.: Effects of Angle of Attack on Transonic Flutter of a Supercritical Wing. Journal of Aircraft, Vol. 20, No. 10, October 1983, pp. 841-847.

29. Farmer, Moses G.: A Two-Degree-of-Freedom Flutter Mount System with Low Damping for Testing Rigid Wings at Different Angles of Attack. NASA Technical Memorandum 83302, 1982.

30. Howarth, L.: On the Solution of the Laminar Boundary Layer Equations. Proceedings of the Royal Society A, London, 1938, p. 164.

31. Fromm, J. E.: and Harlow, F. H.: Numerical Solution of the Problem of Vortex Street Development. Physics of Fluids, Vol. 6, No. 7, 1963.

32. Borland, C. J.; and Rizzetta, D. P.: Nonlinear Transonic Flutter Analysis. AIAA Journal, Vol. 20, No. 11, November 1982, pp. 1606 - 1615.

33. Batina, John T.; Seidel, David A.; Bland, Samuel R.; and Bennett, Robert M.: Unsteady Transonic Flow Calculations for Realistic Aircraft Configurations. AIAA Paper 87-0850, 1987.

34. Batina, J. T.: Unsteady Transonic Flow Calculations for Wing/Fuselage Configurations. AIAA Journal, Vol. 23, No. 12, December 1986, pp. 897 - 903.

35. Tijdeman, H.; Van Nunen, J. W. G.; Kraan, A. N.; Persoon, A. J.; Poestkoke, R.; Roos, R.; Schippers, P.; and Siebert, C. M.: Transonic Wind Tunnel Tests on an Oscillating Wing with External Stores. AFFDL-TR-78-194, 1978.

36. Steinhoff, John; and Jameson, Antony: Multiple Solutions of the Transonic Potential Flow Equation. AIAA Journal, Vol. 20, No.z11, November 1982, pp. 1521 - 1525.

37. Salas, M. D.; and Gumbert, C. R.: Breakdown of the Conservative Potential Equation. AIAA Paper 83-0367, 1983.

38. Gibbons, M. D.; Whitlow, W., Jr.; and Williams, M. H.: Nonisentropic Unsteady Three Dimensional Small Disturbance Potential Theory. AIAA Paper 86-0863, 1986.

39. Whitlow, Woodrow, Jr.; Hafez, Mohamed M.; and Osher, Stanley J.: An Entropy Correction Method for Unsteady Full Potential Flows with Strong Shocks. AIAA Paper 86-1768-CP, 1986.

40. Hafez, M.; and Lovell, D.: Entropy and Vorticity Corrections for Transonic Flows. AIAA Paper 83-1926, 1983.

41. Whitlow, Woodrow, Jr.: XTRAN2L: A Program for Solving the General-Frequency Unsteady Transonic Small Disturbance Equation. NASA TM 85723, 1983.

42. Landon, R. H.: NACA 0012. Oscillatory and Transient Pitching. Compendium of Unsteady Aerodynamic Measurements, AGARD Report No. 702, 1982.

43. Hess, Robert W.; Seidel, David A.; Igoe, William B.; and Lawing, Pierce L.: Highlights of Unsteady Pressure Tests on a 14 Percent Supercritical Airfoil at High Reynolds Number, Transonic Condition. AIAA Paper 87-0035, 1987.

44. Rumsey, C. L.: Time-Dependent Navier-Stokes Computations of Separated Flows Over Airfoils. AIAA Paper 85-1684, 1985.

45. Thomas, J. L.; Taylor, S. L.; and Anderson, W. K.: Navier-Stokes Computations of Vortical Flows over Low Aspect Ratio Wings. AIAA Paper 87-0207, 1987.

46. Kjelgaard, Scott O.; Sellers, William L. III; and Weston, Robert P.: The Flowfield Over A 75 Degree Swept Delta Wing At 20.5 Degrees Angle Of Attack. AIAA Paper 86-1775, 1986.

Table 1.–Summary of Integral–Equation Activities.

α Range \ M Range	Subsonic	Transonic	Supersonic
Low (attached flow) w/large control deflection	UTSA SVP	Nonlinear UTSA SVP	UTSA
Moderate (vortex separation) w/large control deflection	UTSA+ Hybrid vortex SVP	Nonlinear UTSA+ Hybrid vortex SVP	
Large (separated flow) w/ or w/o control deflection	SVP SVP	SVP SVP	

```
 |1980                                          1990|
 |    |    |    |    |    |    |    |    |    |      |
 ┌─────────────────────────────────────────────┐
 { Sub/supersonic integral eq. method for complete a/c }
 { Linear                    Nonlinear          }
 └─────────────────────────────────────────────┘
           \
            \
 ┌─────────────────────────────────────────────┐
 { 2D and 3D Transonic methods                  }
 { Small perturb.;  Full potential; Euler eq.; [Navier-Stokes eq.] }
 └─────────────────────────────────────────────┘
              X
 ┌─────────────────────────────────────────────┐
 {        Viscous flow effects                  }
 { Edge separation; B. L. effect; shock/B. L.; [Surface sep.] }
 └─────────────────────────────────────────────┘
```

═══ Deleted from original plan   ☐ Added to original plan
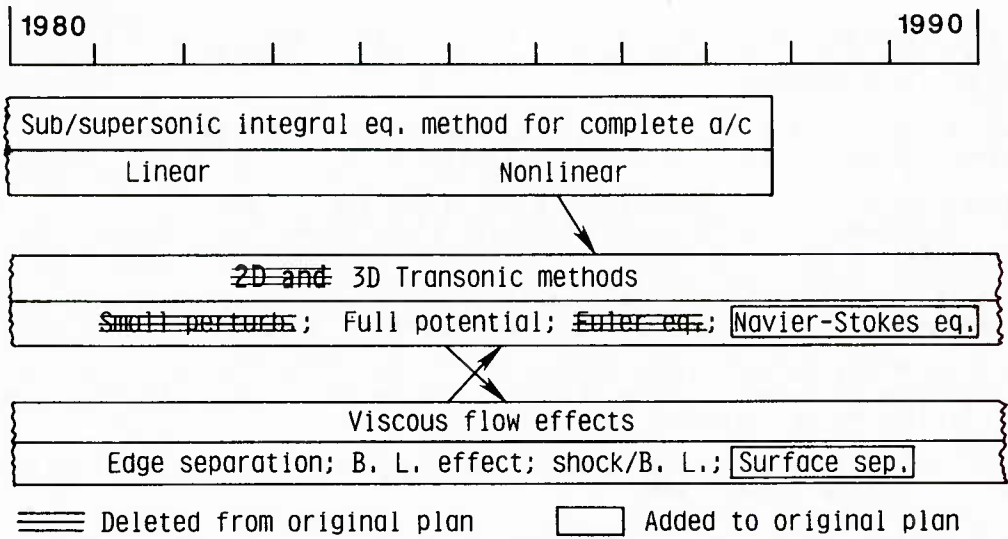
Goal: Validated computational methods for evaluating steady and unsteady loads on aircraft having arbitrary shapes, motions, and deformations (including control surfaces) in subsonic, transonic, and supersonic flow up to high angles of attack

Justification: These methods are needed to evaluate and study structural loads, aerodynamic coefficients, stability character-istics, dynamic loads, and flutter in the analysis and design of advanced high-performance aircraft, including fighters capable of supermanuverability

Fig. 1 - Integral-equation program in unsteady aerodynamics
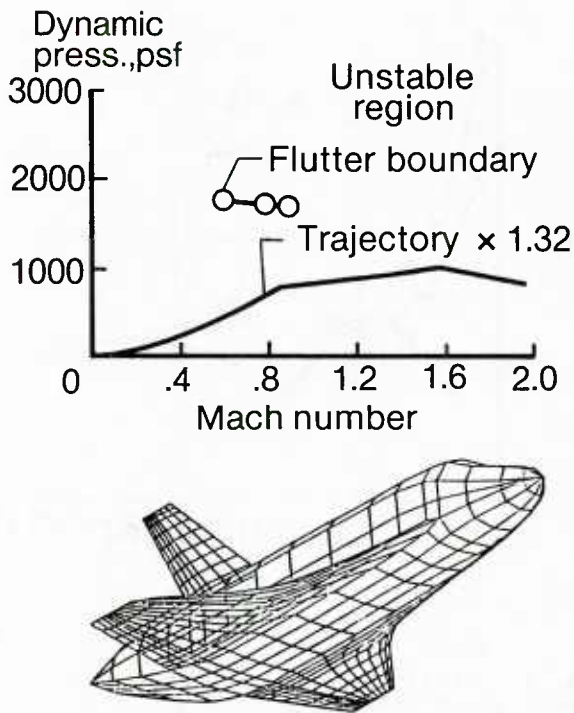
Fig. 2 - Shuttle orbiter flutter analysis
by integral-equation method
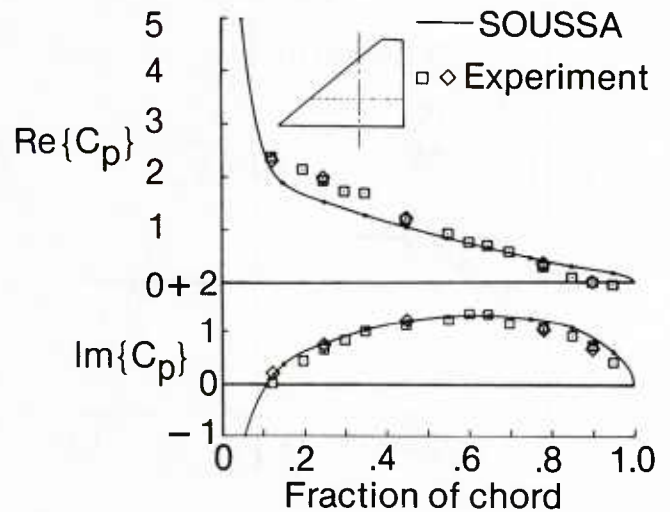
Fig. 3 - Unsteady surface pressures on
clipped-delta wing at Mach number 0.4,
reduced frequency 0.66
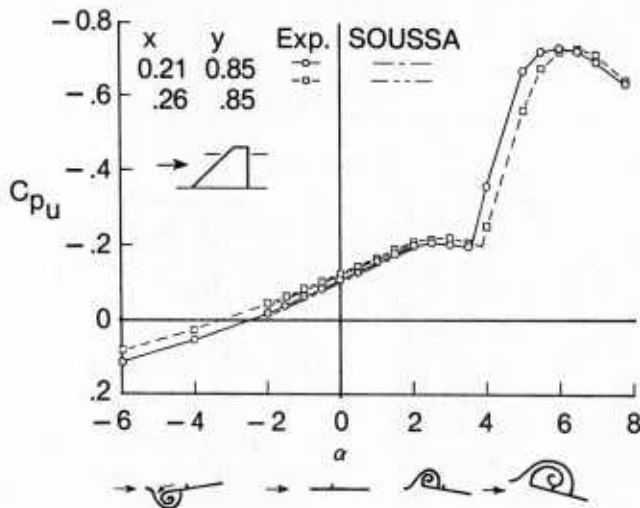
Fig. 4 - Effect of angle of attack on
steady pressures for clipped-delta
wing with 6-percent biconvex airfoil
at Mach number 0.4, Reynolds number $2.\times10^6$
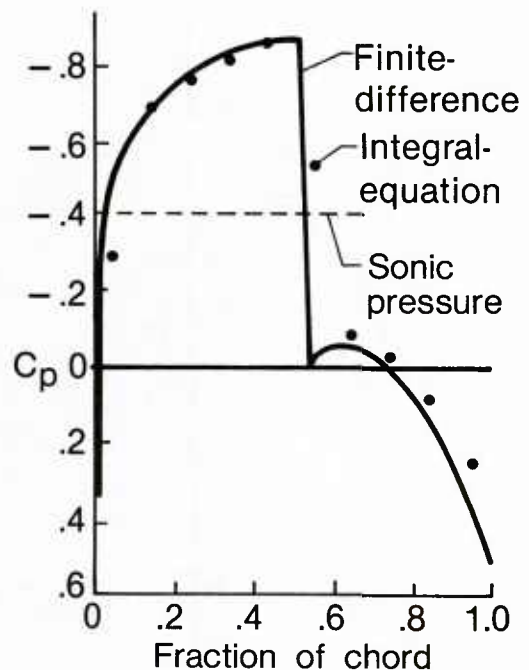
Fig. 5 - Steady pressures near root of
aspect-ratio 6 rectangular wing with
NACA 0012 airfoil at Mach number 0.82,
$\alpha=0$
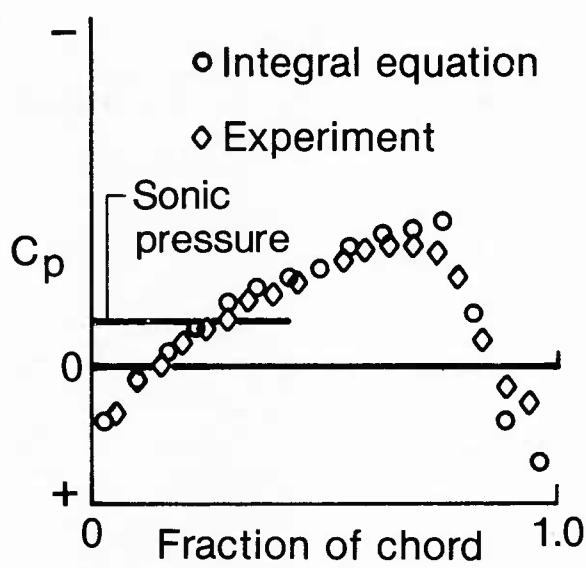
Fig. 6 - Steady pressures for aspect-ratio 4 rectangular wing with 6% bi-convex airfoil at Mach number 0.908, $\alpha=0$
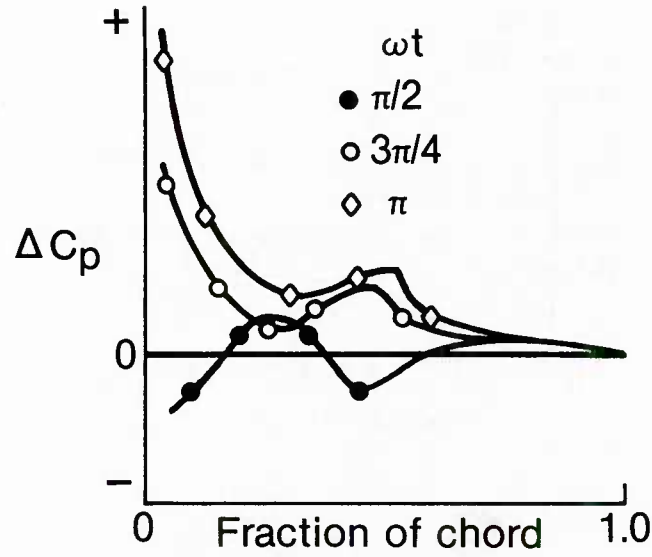
Fig. 7 - Unsteady pressures calculated with SUSAN code for aspect-ratio 5 rectangular wing with NACA 64A006 airfoil pitching at reduced frequency 0.06, Mach number 0.875
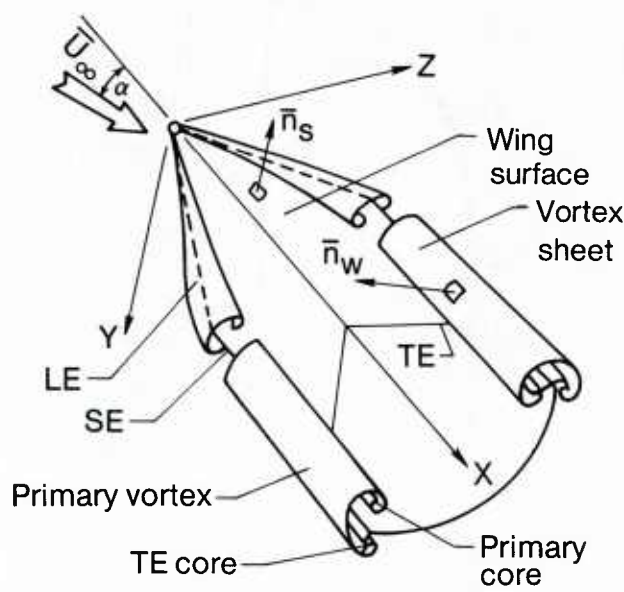
Fig. 8 - Sketch of vortex sheets separating from wing edges
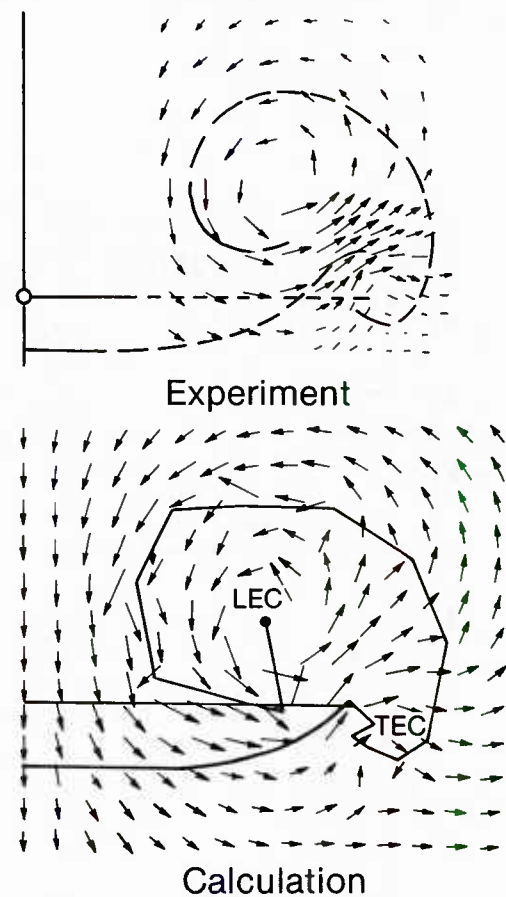
Fig. 9 - Flow field behind aspect-ratio 1 delta wing at $\alpha=20.5^{0}$
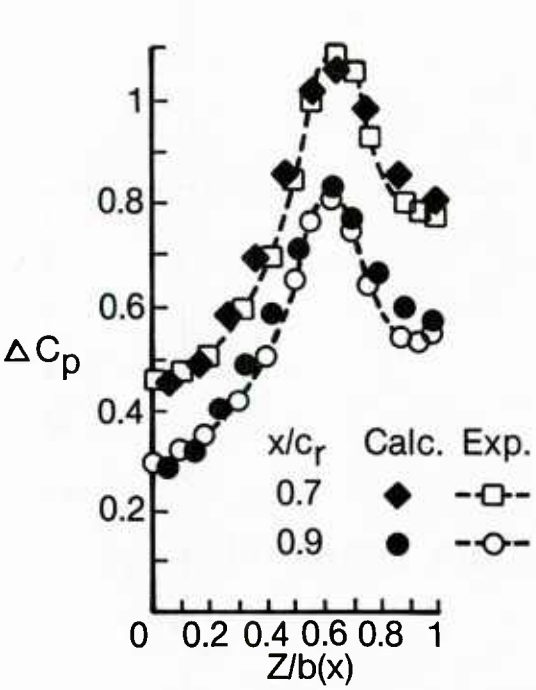
Fig. 10 - Steady pressures on aspect-ratio 1 delta wing at $\alpha=20.5^0$
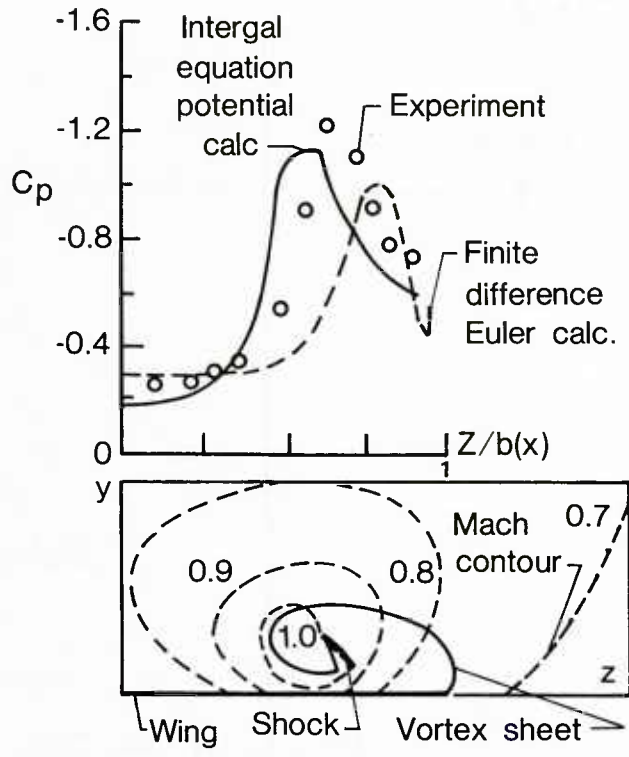
Fig. 11 - Steady pressures on aspect-ratio 1.5 delta wing at Mach number 0.7, $\alpha=15.^0$, $x/c_r=0.8$
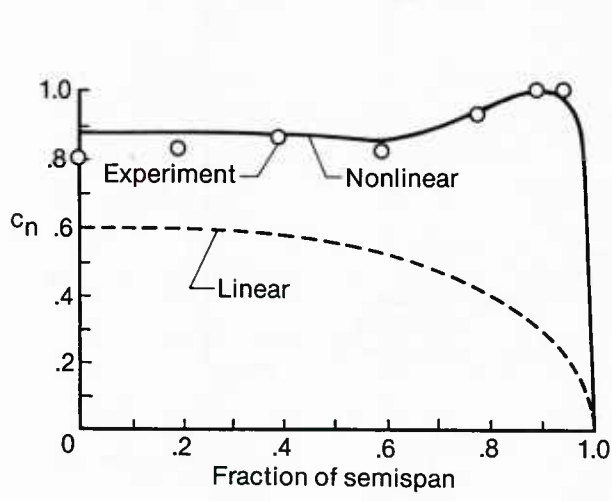
Fig. 12 - Steady spanwise variation of local normal-force coefficient for aspect-ratio 1 rectangular wing at $\alpha=19.4^0$
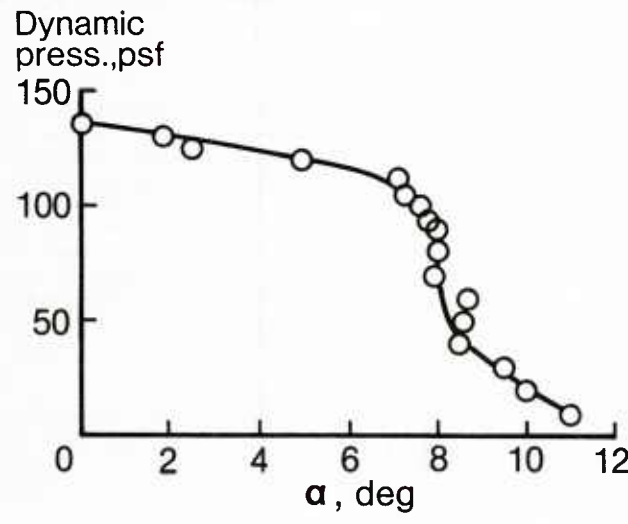
Fig. 13 - Effect of angle of attack on flutter of aspect-ratio-6 rectangular wing with NACA 64A010 airfoil

Distance
from
plate
0.6

Scalar/vector potential

Howarth (ref **30**)

0.0   Velocity, fraction of freestream   1.0
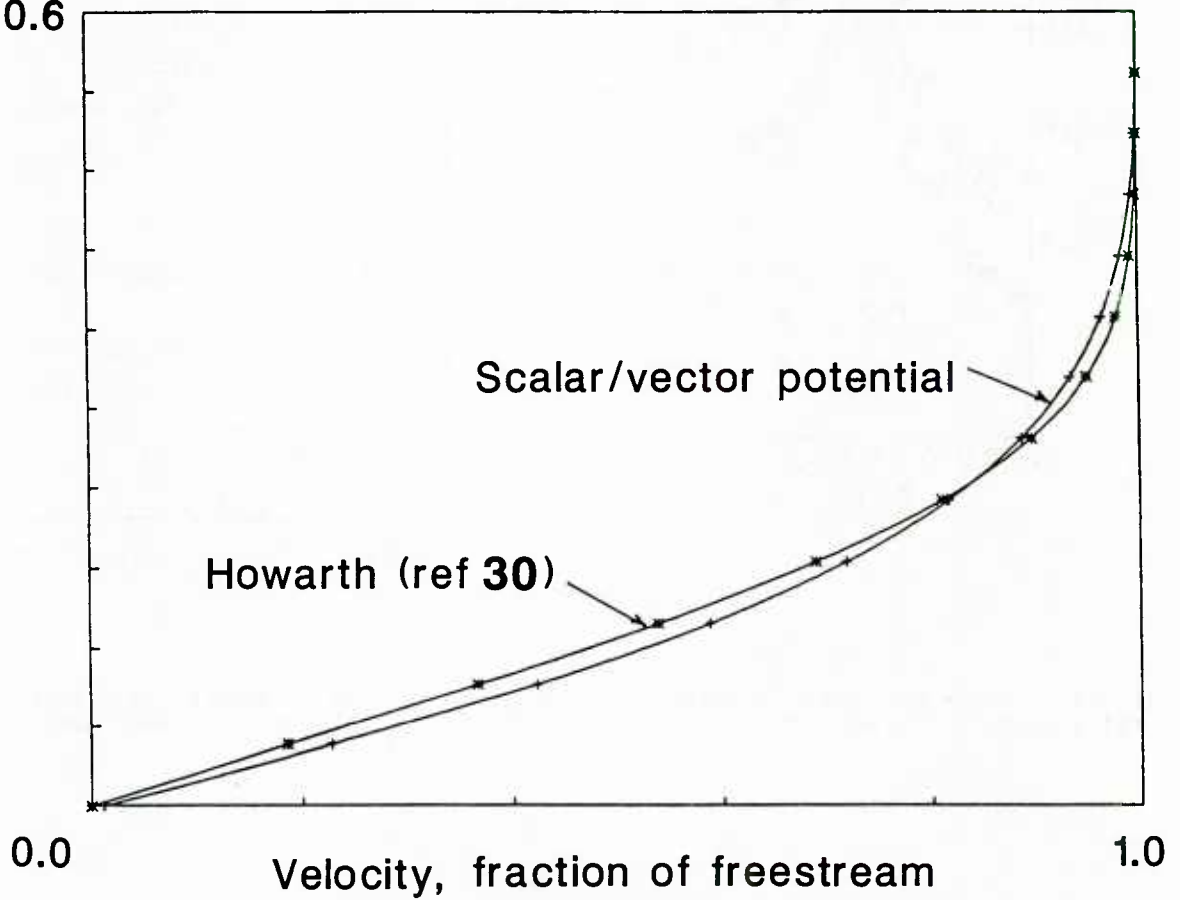
Fig. 14 - Velocity in laminar boundary layer on a flat plate in incompressible flow
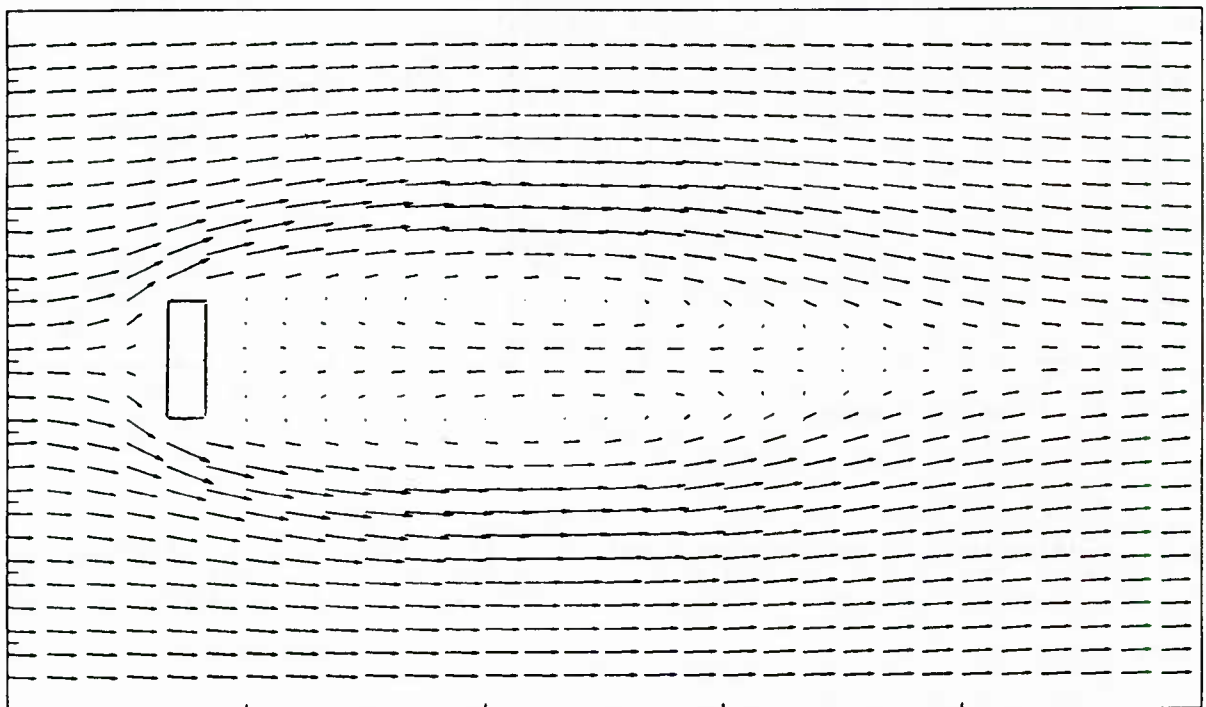
Fig. 15 - Velocity field around a rectangle in incompressible flow
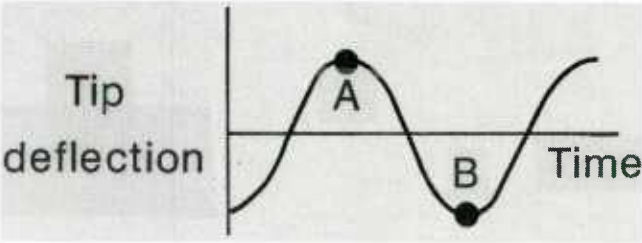
(a) Tip deflection
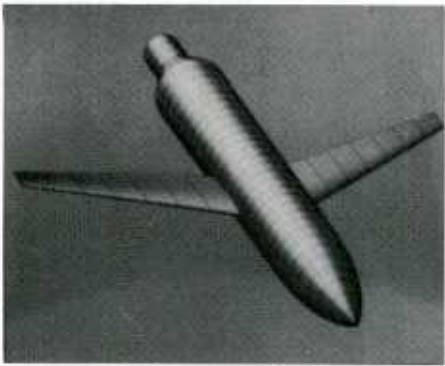
(b) Wing/fuselage gridding
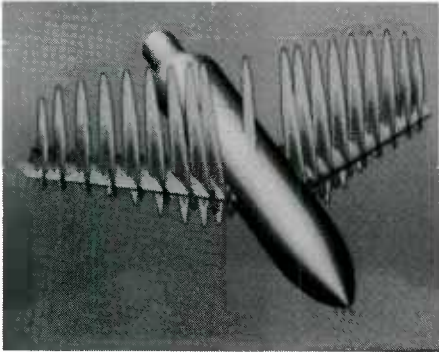
(c) Maximum tip deflection (A)
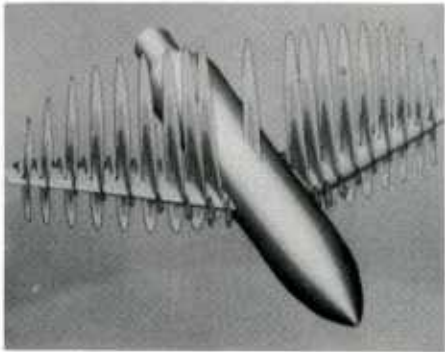
(d) Minimum tip deflection (B)

Fig. 16 - Unsteady transonic calculations for RAE wing/fuselage at Mach number 0.91, α = 1 deg
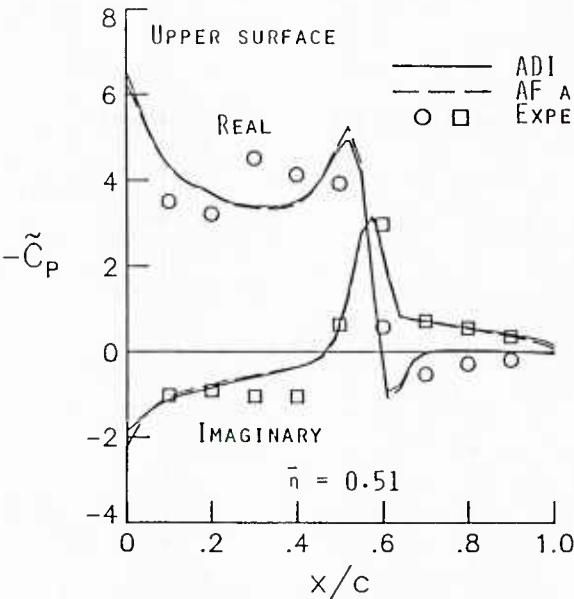
(a) Upper surface
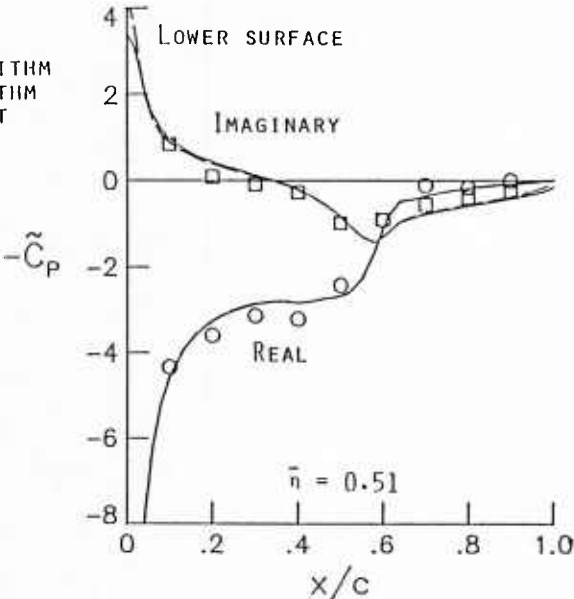
(b) Lower surface

Fig. 17 - First harmonic of unsteady pressures on F-5 wing at Mach number 0.9, α = 0 deg, k = 0.137
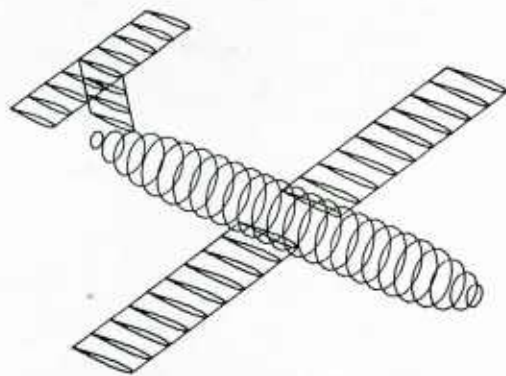
(a) Mathematical model

Fig. 19 - Calculated lift on a rectangular wing with NACA 0012 sections at Mach number 0.82
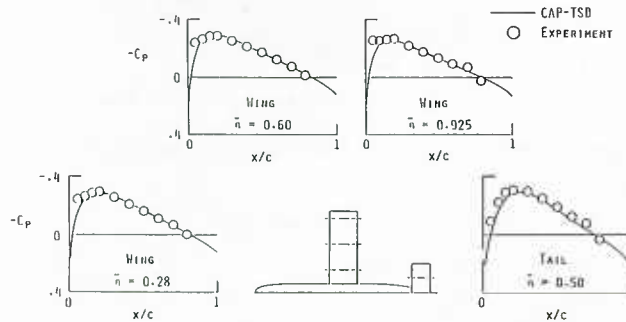
(b) Wing and tail pressures

(a) Isentropic vs. experiment
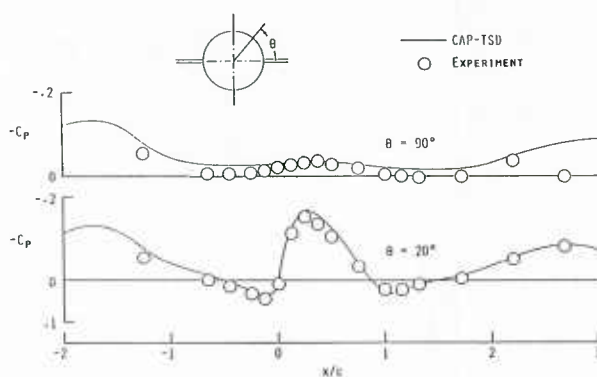
(c) Fuselage pressures

Fig. 18 - Steady flow computations for DFVLR model at Mach number 0.2, $\alpha = 0.15$ deg
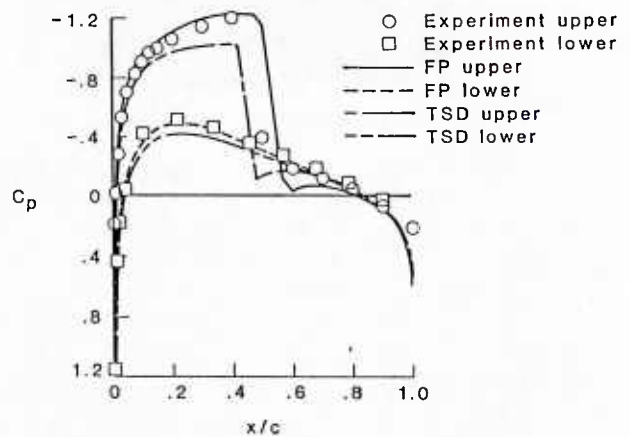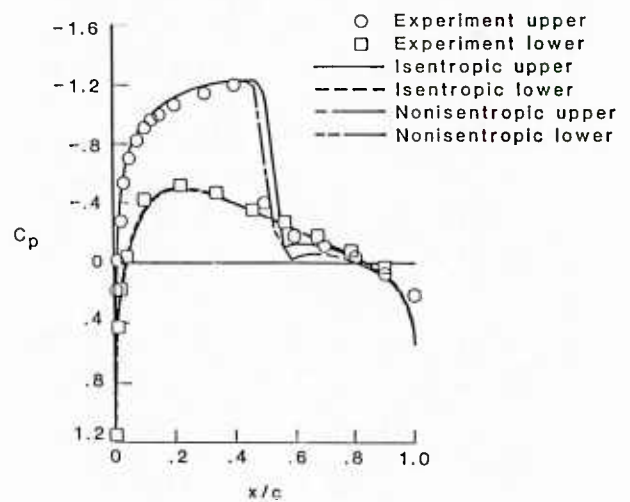
(b) Isentropic and nonisentropic vs. experiment

Fig. 20 - Unsteady pressures on an NACA 0012 airfoil at Mach number 0.755, $\alpha(t) = (0.016 + 2.51\sin(kt))$ deg, $kt = 168$ deg
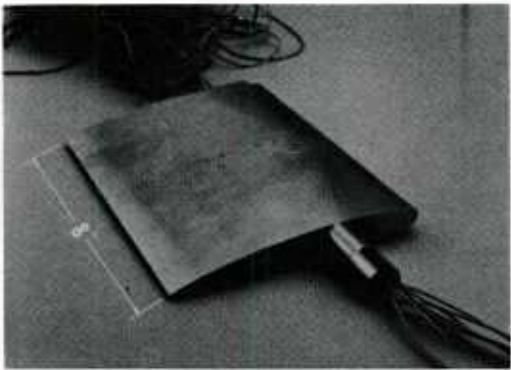
(a) Model
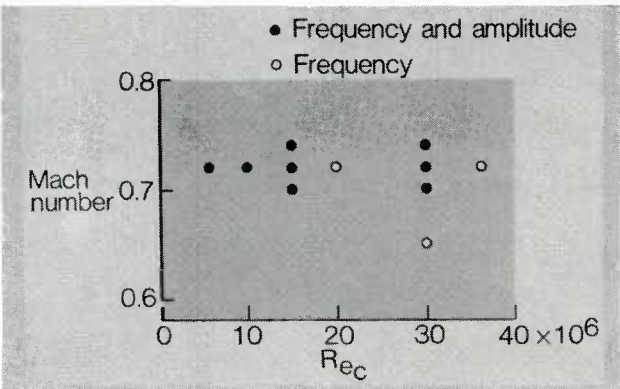
(b) Test conditions
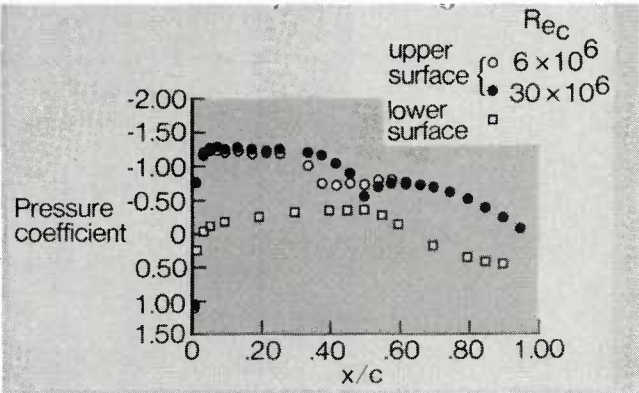
(c) Steady pressure distributions at Mach number 0.72, α = 1.5 deg

Fig. 21 - Study of Reynolds number effects on unsteady pressures
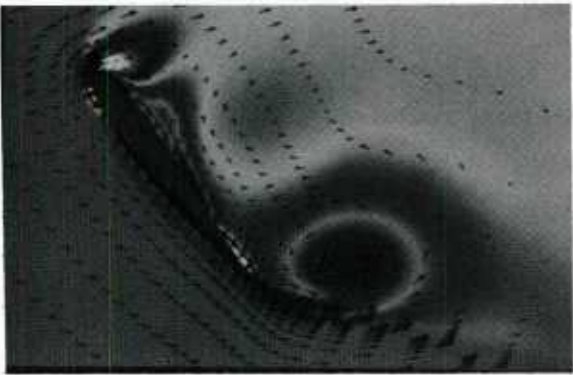
(a) Minimum lift
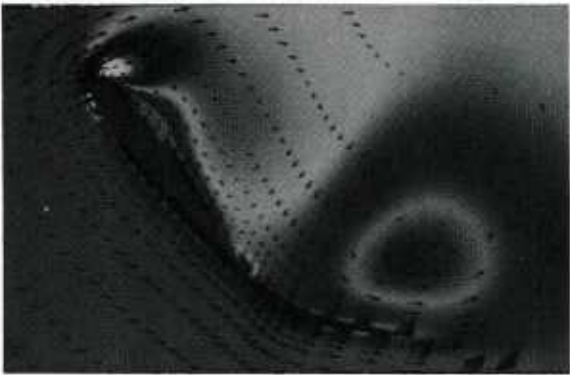
(b) Increasing lift
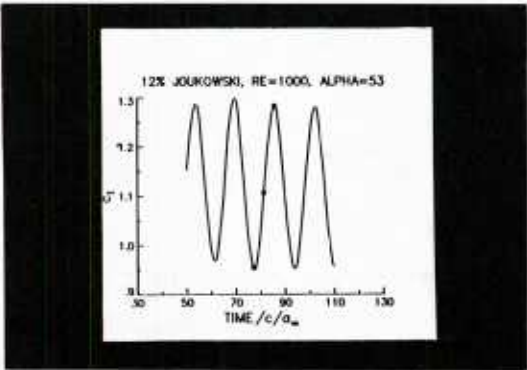
(c) Lift history

(d) Maximum lift

Fig. 22 - Computation of two-dimensional flow separation
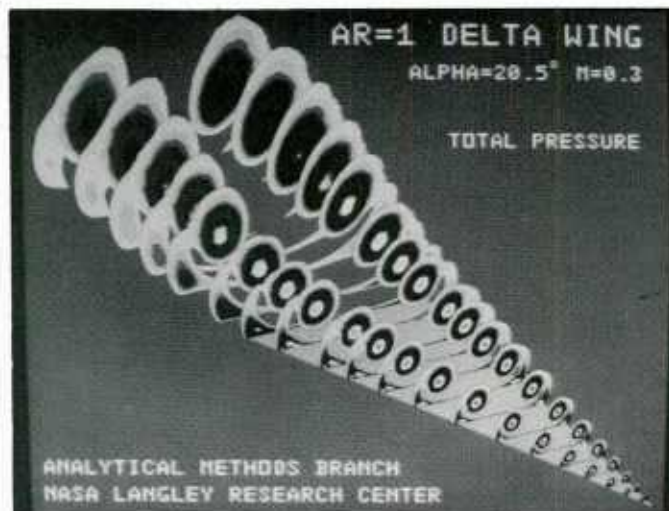
Fig. 23 - Calculated total pressure contours
on a 75 deg delta wing at Mach number
0.3, α = 20.5 deg, Reynolds number = 0.95
million
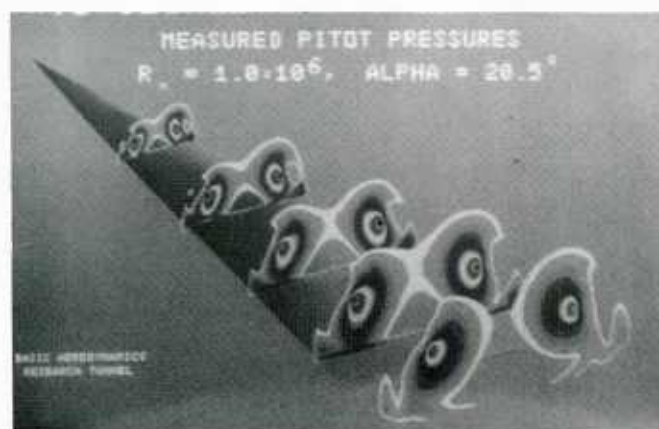
Fig. 24 - Measured total pressure contours
on a 75 deg delta wing at Mach number 0.3,
α = 20.5 deg, Reynolds number = 1 million

CONFIGURATION EQUATION LEVEL	AIRFOIL	WING	WING/BODY	COMPLETE AIRCRAFT
TRANSONIC SMALL PERTURBATION		X	X	X
FULL POTENTIAL		X	X	
EULER/ NAVIER-STOKES	X	X		

Fig. 25 - Summary of finite-difference activities

COMPARISON BETWEEN 2D TRANSONIC FLUTTER CALCULATIONS
IN THE TIME AND FREQUENCY DOMAIN
by
Helmut Zimmermann
Bernd Schulze
Messerschmitt-Bölkow-Blohm GmbH
D-2800 Bremen
Germany

SUMMARY

Unsteady airloads in the transonic speed range for the application in flutter calculations can only be predicted by using nonlinear flow equation codes. In this paper a typical section with the MBB-A3 profile is used as theoretical model for the flutter investigations. Flutter calculations are presented using the classical method in the frequency domain as well as a structural-aerodynamic coupling procedure in the time domain. The unsteady aerodynamic coefficients which are used for these flutter investigations are calculated for several M-numbers and incidences with the TSP-equation without and with quasiunsteady boundary layer and with the time linearized TSP equation without and with steady boundary layer and for comparison reasons with the Doublet Lattice method.

The boundary layer influences essentially the unsteady aerodynamic pressure distributions and coefficients. Mainly for small reduced frequencies, the coefficients calculated with TSP deviate strongly from the coefficients calculated with Doublet Lattice, but the quasiunsteady boundary layer reduces these differences significantly. The results achieved with linearized TSP behave similarly, but with smaller differences compared to TSP. The flutter speeds calculated with TSP airloads show the expected dip in comparison to the Doublet Lattice airloads. The dip over the transonic M-number range is reduced in the range of higher flutter frequencies. But the boundary layer also reduces the dip considerably. The boundary layer also can raise the flutter speed above the Doublet-Lattice values for M-numbers higher than the design M-number when the boundary layer influence changes the flutter frequency.

The flutter results obtained in the frequency and time domain differ less from each other. Nevertheless the time marching flutter simulation takes the nonlinearity effects of the airloads dependent on the vibration amplitude essentially better into account than the classical flutter solution.

1. INTRODUCTION

Since the publication of Farmer and Hanson [1] it became apparent that flutter calculation results in the transonic speed range were nonconservative in comparison to the realistic ones when obtained with unsteady airloads calculated by linear theories, especially for wings with modern profiles. Since that time there has been extensive progress in transonic unsteady computational aerodynamics for application to flutter analysis [2]. But the application of inviscid transonic codes for flutter calculations did not improve the situation. In the range of small shocks the description of the inviscid unsteady flow by an Euler code offered no advantages over the TSP code [2], [3]. More realistic flutter results were obtained by taking into account viscous effects on the unsteady airloads by profile contour changes due to boundary layer displacement thickness and shock-boundary layer interaction. In unsteady aerodynamics viscous effects are at least as important as in steady aerodynamics, because they not only affect the shock position and strength, but also the extent of shock movement.

In contrast to unsteady pressure distributions of linear aerodynamic theories the unsteady pressure distributions obtained in the transonic speed range depend on the mean incidence of the profile and of the amplitude of its motion. Additionally the unsteady pressure distribution induced by harmonic motion of the profile does not behave harmonically but only periodically, i.e. such an unsteady pressure distribution contains higher harmonics for a harmonic motion of the profile.

The flutter solutions in the frequency domain employ only the first harmonic of the airloads for each vibration mode in an eigenvalue analysis to determine the flutter point. By using time marching codes for producing these airloads the airfoil is forced to oscillate in the prescribed mode at the desired frequency until the transients have decayed and a periodic solution is achieved. After Fourier analysis of the time histories only the first harmonic is used in the flutter calculation. The results for different oscillation modes are superposed in the solution process to represent the airloads due to the flutter mode.

In the time domain flutter simulation the structural and aerodynamic equations are coupled and the complete system is time-marched from a prescribed excitation. The stability is assessed from the growth or the decay of the transient response. With this method the higher harmonics of the airloads and the influence of different forms of disturbances on the stability behaviour can be taken into account and superposition of modes is no longer necessary.

In this paper flutter calculation results are shown for a typical section with the MBB-A3 profile, see also [4], [7]. For the calculation of the airloads a finite difference TSP code is used which was developed by the ONERA [5]. For the flutter calculation in the frequency domain the airloads were calculated for various reduced frequencies with the TSP-equation as well as with a time linearized TSP-equation. Viscous effect have been taken into account by an integral boundary layer method [6],[8]. After each time step of the TSP calculation a boundary layer calculation was performed.

2. AERODYNAMIC TOOLS

For the inviscid flow computation the TSP-equation for the velocity potential:

$$M^2 k^2 \varphi_{tt} + 2 M^2 k \varphi_{xt} = \frac{\partial}{\partial x}\left(\beta^2 \phi_x - \frac{\lambda}{2} \phi_x^2 \right) + \phi_{yy} \tag{1}$$

with

$$\lambda = (\gamma + 1) M^2 \tag{1a}$$

is solved using an ADI Finite-Difference-Scheme. The procedure was established by [5].

The boundary conditions on the airfoil: $y=f(x,t)$ and on the wake are:

$$\phi_y = f_x + f_t + d_x \qquad \text{on the airfoil} \tag{2}$$

$$\Delta \phi_y = \Delta d_x \tag{3a}$$
$$\Delta \left(\phi_x + \phi_t \right) = 0 \qquad \text{across the wake} \tag{3b}$$

d means the boundary layer displacement thickness and Δ indicates the jump $(+y \to 0) - (-y \to 0)$

For the pressure derivative the linearized expression

$$C_p = -2 \left(\phi_x + \phi_t \right) \tag{4}$$

is used. Across the wake

$$\Delta C_p = 0 \tag{4a}$$

For the time linearized version of the TSP-equation:

$$M^2 k^2 \varphi_{tt} + 2 M^2 k \varphi_{xt} = \frac{\partial}{\partial x}\left(\beta^2 \varphi_x + \lambda \phi_x^0 \varphi_x \right) + \varphi_{yy} \tag{5}$$

with the steady potential ϕ^0 the same solution procedure is applied as for the TSP-equation.

A steady integral method [6] is used for the boundary layer calculation. Usually for the calculation of the boundary layer displacement thickness an iterative inviscid-viscid coupling procedure is used. For this procedure the velocity distribution of the last time step is used as boundary condition for the calculation of the next time step of the displacement thickness (Fig. 1). But in the vicinity of the inviscid separated flow region one of the boundary layer equations become singular. Therefore for the separated flow region an indirect solution of the boundary layer equation is used; that means an estimated boundary layer displacement thickness is calculated by an inverse procedure and in each iteration step the velocity distribution of the inviscid region is compared with the velocity distribution of the viscid region by an relaxation formula (Fig. 2). In this paper the Carter relaxation formula is applied.

For the calculation of the unsteady pressure distribution including the boundary layer the following three phases for the time marching process are used:

1. For the steady pressure distribution calculation with the TSP-equation the real profile is blown up from the flat plate in about 80 iteration steps.

2. After that the steady boundary layer displacement thickness is added in an alternating process to the geometrical profile thickness. This process needs 30 up to 70 time steps.

3. After the steady phase is finished the harmonic excitation of the profile is started. For each time step only one viscid-inviscid calculation is made, as long as the boundary layer calculation does not diverge. No unsteady terms are applied in the boundary layer equation.

Fig. 4 shows the growth of the boundary layer displacement thickness with the increasing number of iteration steps for the steady case of the MBB-A3 profile (Fig. 3) for M=0.8, α=-0.2° and Re=17.7 10^6. The ramp in the boundary layer displacement thickness in front of the shock position is visible. The triangle shows the laminar-turbulent transition point. The cross indicates the chordwise downstream position at which the direct boundary layer calculation was replaced by the indirect one.

Fig. 5 shows the steady and unsteady pressure distribution of a TSP calculation without and with boundary layer. The steady parameters are the same as in Fig. 4 (M=0.80, α=-0.2° Re=17.7 10^6) for the reduced frequency of k=0.104. The result of an Euler calculation without boundary layer for the same flow parameters is added. The results for the steady and unsteady pressure distributions for TSP without boundary layer and Euler agree well. The large influence of the boundary layer on the pressure distribution is clearly visible.

Aeroelastic Equation of Motion

The classical flutter calculation is based on a modal representation of the structure. The elastic displacements are developed in a series of structural eigenmodes :

$$f(x,t) = \sum_{i=1}^{N} \Psi_i (x) q_i(t) \tag{6}$$

For a two-degree of freedom case this representation is exact for N=2. The structural equation of motion then reads:

$$M_i \ddot{q}_i + K_i q_i = Z_i(t)$$ (7)

q_i - generalized coordinates
M_i - generalized masses
K_i - generalized stiffness
Z_i - generalized aerodynamic forces

$$Z_i(t) = \frac{1}{2}\rho V^2 \int \Delta p(t) \, \psi_i \, dF$$ (8)

For the flutter calculation in the frequency domain only the first harmonic of the airloads induced by a pure harmonic motion is taken into account. The generalized aerodynamic forces are supposed to be linear functions of the generalized coordinates and thus can be superposed:

$$Z_i(t) = \sum_{j=1}^{N} A_{ij}(\omega) \, \bar{q}_j \, e^{i\lambda t}$$ (9)

with

$$A_{ij} = \frac{1}{2}\rho V^2 \int \Delta p_j(\omega) \, \psi_i \, dF$$ (9a)

In this way the differential equation (7) can be transformed into an eigenvalue problem

$$[-\lambda^2 M + K - A(\omega)]\bar{q} = 0$$ (10)

with

$$i\lambda = \delta + i\omega$$ (10a)

The implicit dependence $A(\omega)$ only allows an iterative solution process. In this paper the flutter calculations are performed with the p-k method [9].

For the flutter simulation in the time domain equation (7) is solved directly. This approach is not restricted by linear assumptions of the aerodynamic forces. In this paper flutter simulation results are obtained using a Newmark integration [10]. The equation of motion (7) then reads:

$$q^{n+1} = [a_0 M + K]^{-1} [Z^{n+1} + a_0 M q^n + a_2 M \dot{q}^n + a_3 M \ddot{q}^n].$$ (11a)

$$\ddot{q}^{n+1} = a_0 (q^{n+1} - q^n) - a_2 \dot{q}^n - a_3 \ddot{q}^n$$ (11b)

$$\dot{q}^{n+1} = \dot{q}^n + a_6 \ddot{q}^n + a_7 \ddot{q}^{n+1}$$ (11c)

with

a_i - integration constants
n - time step index

The aerodynamic forces at the time level n+1 are still unknown when solving equation (11a). Thus those of time level n are introduced. This causes the phase shift of one time step which can be neglected for sufficient small time steps.

Frequency and damping estimates are determined fitting the time responses by complex exponential functions of the form:

$$q(x,t) = a_0 + \sum_{i=1}^{N} e^{\delta_i t} [a_i \cos \omega_i t + b_i \sin \omega_i t]$$ (12)

A least squares curve fitting procedure is employed following an optimization algorithm of Jacob [11].

3. RESULTS AND DISCUSSION

Overview

Flutter calculation were established for a typical section with an MBB-A3 profile (Fig. 3). Steady pressure distributions in the M-number range between M=0.756 and M=0.82 were calculated with the TSP-equation for various incidences. Unsteady pressure distributions for the same M-number and incidence range were calculated in a reduced frequency range between 0.05 and 0.5 for pitch and heave motion. It was striking that the solutions for unsteady pressure distributions for M-numbers higher than M=0.8 diverged in most cases although the steady shock was not positioned at the trailing edge of the profile. Solutions with the time linearized TSP-equation for selected cases were also established. For these cases the necessary steady potential was calculated with the TSP-equation. For some cases the steady and unsteady pressure distributions were calculated including the steady and quasi-unsteady boundary layer. For the calculation of the unsteady pressure distribution with the linearized TSP-equation including the boundary layer only the boundary layer for the steady potential was taken into account. The following abbreviations are used for the aerodynamic results.

D.L................Doublet Lattice
TSP................Transonic small perturbation
lin. TSP...........Time linearized TSP
visc. TSP..........TSP with quasiunsteady boundary layer
visc. lin. TSP.....Time linearized TSP with steady boundary layer

Because the solutions with the term Φ_{tt} in the TSP-equation showed disturbances this term was neglected. This neglect is without an influence on the flutter results, because the reduced flutter frequencies of the performed flutter calculations were smaller than k=0.3. From the first harmonic of the unsteady pressure distributions the force- and moment-coefficients were derived. The unsteady aerodynamic coefficients with D.L. and for the plate with a purely elliptic flow field with TSP were calculated for reasons of comparison.

Steady Aerodynamic Results

Fig. 6 shows the steady pressure distributions for M=0.765 and α=1.5° calculated with the TSP equation including the boundary layer effect in comparison with A.R.A. measurements. The calculated pressure distribution fits the measured one well. The pressure distribution calculated by TSP (matching the M-number and the incidence) does not fit as well to the measured one as the visc. TSP solution which was not matched. But the boundary layer effect on the steady pressure distribution can only approximately be represented by inviscid calculations and changed parameters.

Fig. 7 shows the steady pressure distribution for M=0.78 and α=1.3° calculated with TSP and visc. TSP. The pressure distribution without boundary layer has a more downstream shock position and a higher pressure rise at the shock than the pressure distribution including the boundary layer, resulting in a reduction of steady lift in the latter case. The visc. TSP solution can approximately be matched by TSP when reducing the incidence to α=0.75°.

Unsteady Aerodynamic Results

Fig. 8 and Fig. 9 shows the unsteady pressure distribution for M=0.756 and α=1.3° with a pitch amplitude of 0.5° for the reduced frequency range 0.1 to 0.5 calculated with TSP and visc. TSP respectively. The peaks in the unsteady pressure distributions on the upper side near the steady shock positions are strongly decreased and shifted upstream by the boundary layer effect. But even the levels of the pressure fore and aft of the peaks are changed.

Fig. 10 shows the unsteady pressure distribution calculated for M=0.78, α=1.3° and a pitch angle of 0.5° and a reduced frequency of k=0.2 with TSP and visc. TSP. The unsteady pressure distribution for α=0.75° calculated without boundary layer is shown for comparison. The latter does not fit the unsteady pressure distribution calculated with TSP including boundary layer as well as the steady pressure distribution do under the same conditions (see also Fig. 7).

Fig. 11 shows the unsteady pressure distribution for M=0.78; α=0.5°; reduced frequency of 0.2, and a pitch amplitude of 0.5° calculated with TSP and Lin. TSP. For the TSP solution the peaks on the upper side induced by the shock are a little more downstream than for the Lin. TSP solution. This effect can be produced by the asymmetric shock motion about the steady shock position in the TSP solution.

Fig. 12 shows the unsteady pressure distribution for the same flow parameters calculated with visc. TSP and visc. Lin. TSP. The pressure distributions on the upper and lower surface are well comparable. The peaks of the pressure distribution in the vicinity of the shock on the upper surface calculated with visc. Lin. TSP are a little higher than of the pressure distribution calculated with visc. TSP. This effect is valid for all comparisons for pressure distributions, calculated in the above mentioned way.

Fig. 13 shows the unsteady aerodynamic coefficients for M=0.756 and α=1.3° and a range of reduced frequencies between 0.05 and 0.5. A pure elliptic solution of the TSP code for the flat plate is indicated in addition to the above mentioned methods. These coefficients are also derived from the first harmonic of the unsteady pressure distributions. The upper part of the figure shows the coefficients for the pitch motion and the lower part those for the heave motion. Because of the neglect of the Φ_{tt}-term in the TSP equation there exists a small discrepancy for "higher" reduced frequencies between D.L. and flat plate results. The largest difference exists beween D.L. and TSP results. With the exception of the imaginary part of Cm_α and the real part of Cm_h the magnitude of the difference between the different results and D.L. decreases in the sequence TSP, Lin. TSP, visc. Lin. TSP and visc. TSP. The most striking effect is the large difference between TSP and visc. TSP. This difference is on the average larger than between D.L. and visc. TSP. This effect is already indicated in the unsteady pressure distributions.

Fig. 14, 15, and 16 show the unsteady aerodynamic coefficients against frequency for Mach numbers 0.76, 0.78, and 0.80 respectively. Each of the figures shows the values for three angles of attack, calculated with TSP; plus a fourth curve which represents the result of visc. TSP for the highest incidence. Generally the values for the real and imaginary part increase with increasing incidence except for α=1.3° for M=0.78. For M=0.8 this tendency is not as clear as for M = 0.765 and M=0.78. But the TSP code tends to become unstable with increasing incidences. The aerodynamic coefficients calculated with visc. TSP agrees best with the TSP solution for the lowest incidence, confirming the tendency of the boundary layer to reduce the effective incidence.

Flutter Calculation Results

To show the influence on flutter of the different aerodynamic input, a two-dimensional dynamic model was selected. Fig. 17 shows the mode shapes and the eigenfrequencies of this model which are chosen in such a way, that they represent the streamwise motion of a strip in the outer wing section of a backward swept wing of a transport aircraft for the two eigenmodes fundamental bending and engine pitch. Mode 1 is characterized by a large heave and a small pitch motion with a nodal point upstream of the section. x_1^K is the distance between the nodal point and the 1/4 point of the section. Mode 2 is characterized by a pitch motion around a point with a distance x_2^K downstream of the 1/4 point of the section.

The flutter results were obtained for a variable mass ratio corresponding to the condition in a pressurized windtunnel for selected M-numbers at constant stagnation temperature. Therefore the flutter results, frequencies and damping of the different modes, depend on the stagnation pressure for a constant M-number. The most important coefficients for flutter of this representative section are Cl_α and Cl_h as long as the nodal point of the second mode is remote from the 1/4 point of the section. If the nodal point of the second mode is close to the 1/4 point the moment coefficients can also become important for flutter.

For all the cases the mode shapes were chosen in the following way: Mode 1: $x_1^K = -10.$; Mode 2: $x_2^K = 0.5$. The flutter calculation presented in Fig. 18 was performed with a chord length of 0.3 m and in Fig. 19 with a chord length of 0.6 m. That means the reduced frequencies used in Fig. 18 are approximately half the reduced frequencies in Fig. 19.

For the first case (c=0.3 m), the critical stagnation pressures that were calculated for various Mach numbers and incidences are shown on Fig. 18 plotted against Mach number. The Mach number ranges from 0.756 to 0.8, the incidences from 0° to 1.3°, plus a case for M=0.82 and $\alpha = -1°$. The methods that were used to calculate these values were: D.L., TSP, visc. TSP, lin. TSP, visc. lin. TSP.

The Mach number was limited at the lower boundary by the design Mach number, and at the upper end by the breakdown of the TSP code. The upper end of the incidence range was limited by either the breakdown of the TSP code or the onset of one-degree-of-freedom flutter at zero stagnation pressure. The one-degree-of-freedom flutter is induced for this small reduced frequency by the magnitude of the unsteady aerodynamic coefficients: the imaginary part of Cl_α and the imaginary part of Cm_h. In Fig. 18 two flutter cases are involved: one-degree-of-freedom flutter for the bending mode with low critical stagnation pressures, and bending-torsion flutter. The flutter points calculated with the D. L. and visc. TSP codes belong to the bending-torsion flutter type, but the flutter points calculated with the TSP code are strongly influenced by the one-degree-of-freedom flutter.

Therefore at low reduced frequencies the noticeable decrease in critical stagnation pressures, calculated with the inviscid codes, is caused mainly by a change in the flutter type. Nevertheless the curves drawn in Fig. 18 for constant incidence indicate the transonic dip. What is striking here is the large discrepancy between the D.L. solution and the TSP solutions dependent on incidence, compared to the small differences between D.L. and visc. TSP, which are nearly independent of incidence. The flutter point calculated with TSP for M=0.8 and $\alpha = 0.75$ with a higher stagnation pressure as for D.L. is not understandable, but not a failed calculation.

The calculations for the second case (c=0.6 m) were performed with the same aerodynamic input. For this higher reduced frequency range no one-degree-of-freedom flutter influence appears, as in Fig. 18. Therefore the limit for the upper M-number and incidence boundary was defined by the divergence of the TSP code. In Fig. 19 a typical transonic dip is visible for the critical pressure points calculated with the TSP code, which is also due to the dependence on incidence. The critical pressure points calculated with the Lin. TSP with and without the steady boundary layer also show the dip effect in the expected way. But the solutions with visc. TSP show higher values for the critical stagnation pressure for the M-numbers 0.78 and 0.8 than calculated with D.L. This result can be explained by the different behaviour of the pitch frequency vs. stagnation pressure for visc. TSP. It is uncertain whether this effect is realistic since the unsteady terms in the boundary layer were neglected.

Flutter Simulation Results

Fig. 20 shows the typical phases of the flutter simulation approach. In the first part of the steady phase, incidence and profile thickness are increased from zero to full value, to start the calculation. Then the airfoil is held motionless until a steady state is achieved. In the second phase a forced excitation in pitch and heave is applied:

$$\alpha(t) = \bar{\alpha} \sin \omega t$$
$$h(t) = \bar{h} \sin(\omega t + \varphi)$$

Frequency, phase and ratio of amplitudes of the excitation are the same as those of the flutter mode of the flutter calculation. After three cycles the excitation is switched off leaving the section in free vibration. In order to keep the profile in a mean position which corresponds to the steady incidence, an initial stress is added during this phase to compensate the static unbalance. Fig. 20 compares a TSP to a visc. TSP simulation at design conditions. The time responses of the TSP simulation show a slightly unstable development while the visc. TSP responses are well damped.

In Fig. 21 TSP flutter simulation results with three different amplitudes are presented for M=0.756 and $\alpha = 1.3°$. The left side of the figure shows the time responses for a nearly critical stagnation pressure, while on the right hand side a supercritical case is presented. The amplitude growth rates become larger for higher initial excitation amplitudes. The higher harmonics are visible only in the time histories of the moment coefficient.

Fig. 22 and Fig. 23 show the frequency and damping curves vs. stagnation pressure at design conditions for the flutter model with 0.3 m and 0.6 m respectively. Flutter calculation results are compared to flutter simulation results for three different amplitudes. The development of the simulation results agree well with the calculation results. The simulation approach produces flutter at about 5-10% lower stagnation pressures depending on the frequency range and the amplitude ratio. For the 0.3 m case the flutter pressure reduces with increasing amplitudes while for the 0.6 m case the dependence of amplitude is low.

CONCLUSION

For moderate transonic Mach numbers and incidences the steady and unsteady pressure distribution calculated with TSP generally agree well with the corresponding ones calculated with the Euler code. The stability of the TSP code, however, is weak.

While the steady flow solutions are strongly influenced by the boundary layer, the unsteady solutions seem to be affected even more by the boundary layer. Inviscid solutions, which are matched to viscid steady pressure distributions deviate considerably in their unsteady behaviour. Therefore flutter calculations that use airloads calculated by nonlinear methods must take account of boundary layer effects, at least in the case of supercritical profiles or profiles with strong nonlinear variation of Cl with incidence, or if the boundary layer linearizes the Cl vs. incidence variation considerably.

The influence of higher harmonics in the unsteady pressure distribution, and the nonlinear dependence on the amplitude, have a smaller influence on flutter, as shown by the comparison between the results of flutter calculation and flutter simulation.

REFERENCES

[1]   Farmer, M.G., Hanson, P.W.
        Comparison of supercritical and conventional wing flutter characteristics
        AIAA/ASME/SAE 17th Structure,
        Structural Dynamics and Material Conference
        May 1976

[2]   Ballhaus, KW.F., Bridgeman, J.O.
        Numerical Solution Techniques for Unsteady Transonic Aerodynamics Problems
        AGARD Rep. 679, March 1980

[3]   Tijdeman, H.
        Investigations of the transonic flow araound oscillating Airfoils
        NLR TR 77090 U

[4]   Zimmermann, H.,
        Application of Transonic Unsteady Methods for Calculation of Flutter Airloads
        AGARD, Toulouse 1984

[5]   Couston, M., Angélini, J.-J., Mulak, P.
        Application de l'equation des petites perturbations transoniques aux calculs d'ecoulements bidimensionels instationaires
        La Recherche Aerospatiale No. 1979-5, pp. 325-340

[6]   Thiede, P., Elsholz, E., Dargel, G.
        Rationelle Berechnung partieller Ablösegebiete auf der Basis des Grenzschichtkonzepts
        RüFo IV, T/RF41/80050/81449, 1981

[7]   Zimmermann, H., Vogel, S.
        Application of Transonic Unsteady Methods for Calculation of Flutter Airloads
        Second International Symposium on Aeroelasticity and Structural Dynamics
        Aachen 1985

[8]   Dau, K., Schulze, B., Zimmermann, H.,
        Instationäre Luftkräfte im transsonischen Bereich und ihre Auswirkungen auf das Flatterverhalten,
        Teil III
        BMVg-FBWT 86-1

[9]   Vogel, S.
        Ein Beitrag zur Lösung der Flattergleichung unter Berücksichtigung von Servorsteuerung und Flugregler
        ZFW Band 1, Heft 2, 1977

[10]   Bathe, K.-J.
        Finite Element Procedures in Engineering Analysis
        Prentice-Hall, Inc., Englewood Cliffs, New Jersey 07632, 1982

[11]   Jacob, H.G.
        Rechnergestützte Optimierung statischer und dynamischer Systeme
        Springer-Verlag, Berlin, Heidelberg, New York, 1982
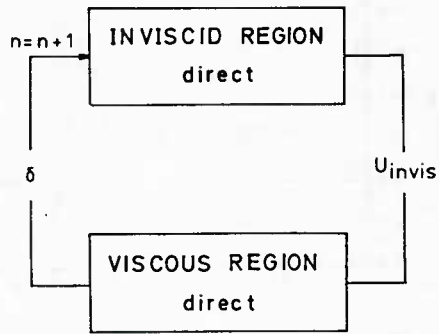
Fig. 1 Direct viscid—inviscid
coupling procedure
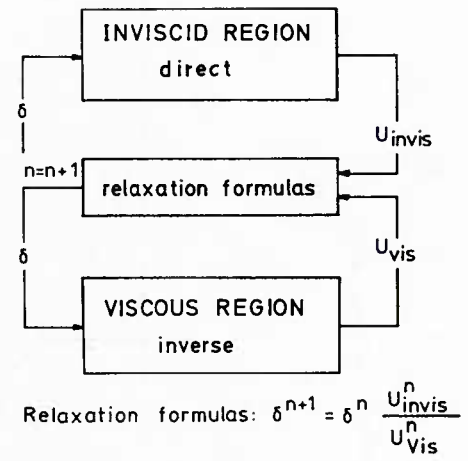
Fig. 2 Indirect viscid—inviscid
coupling procedure

Relaxation formulas: $\delta^{n+1} = \delta^n \dfrac{U^n_{invis}}{U^n_{Vis}}$
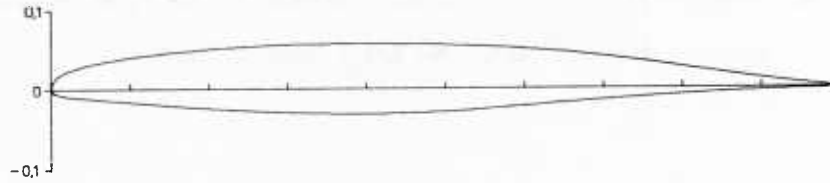
Fig. 3 MBB—A3 profile

ITER. 80-95
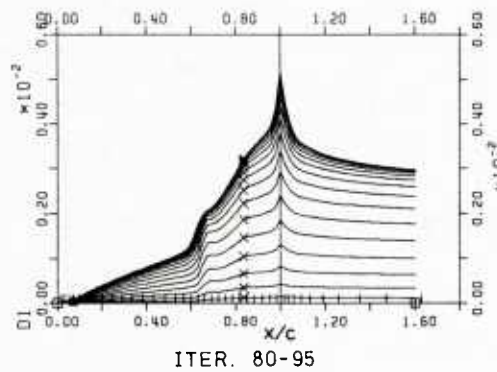
Fig. 4 Iterative development of the boundary layer displacement thickness
MBB—A3, M=0.8, $\alpha=-0.2^0$ and Re=17.7 10^6
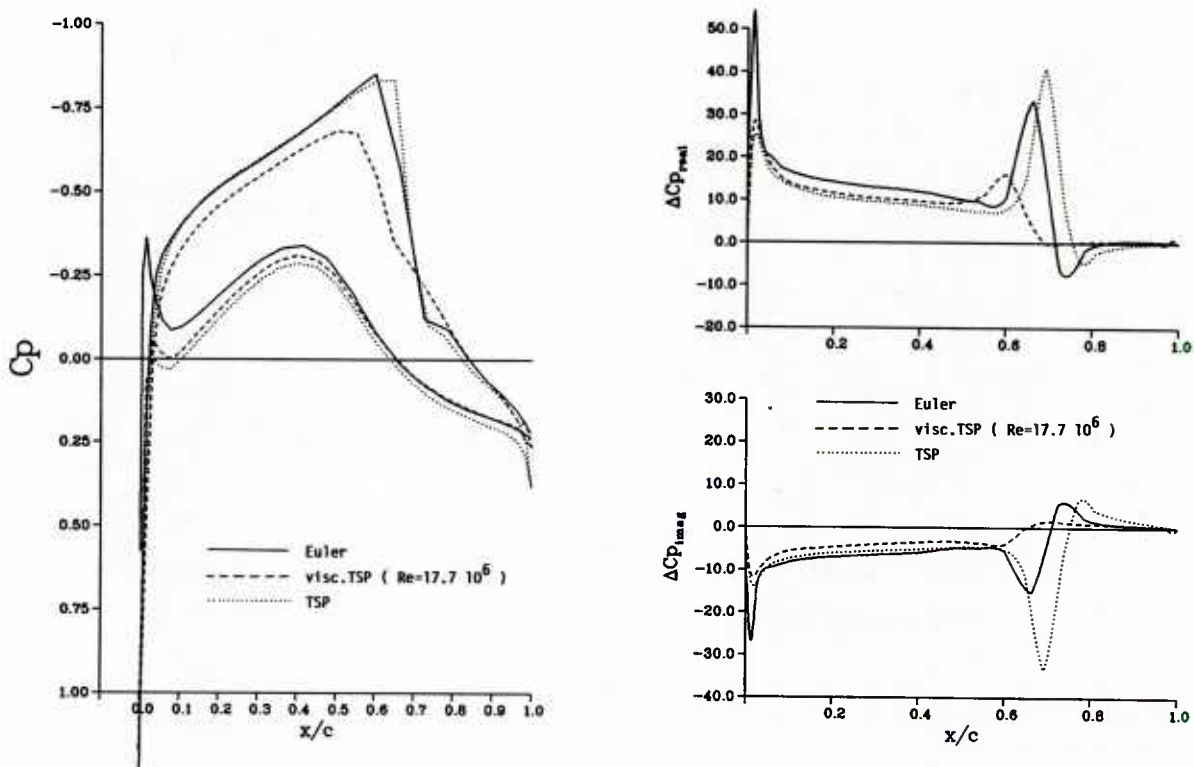
Fig. 5 Steady and unsteady pressure distribution for MBB–A3 profile
M=0.8, α=−0.2° and k=0.104 (pitch motion)
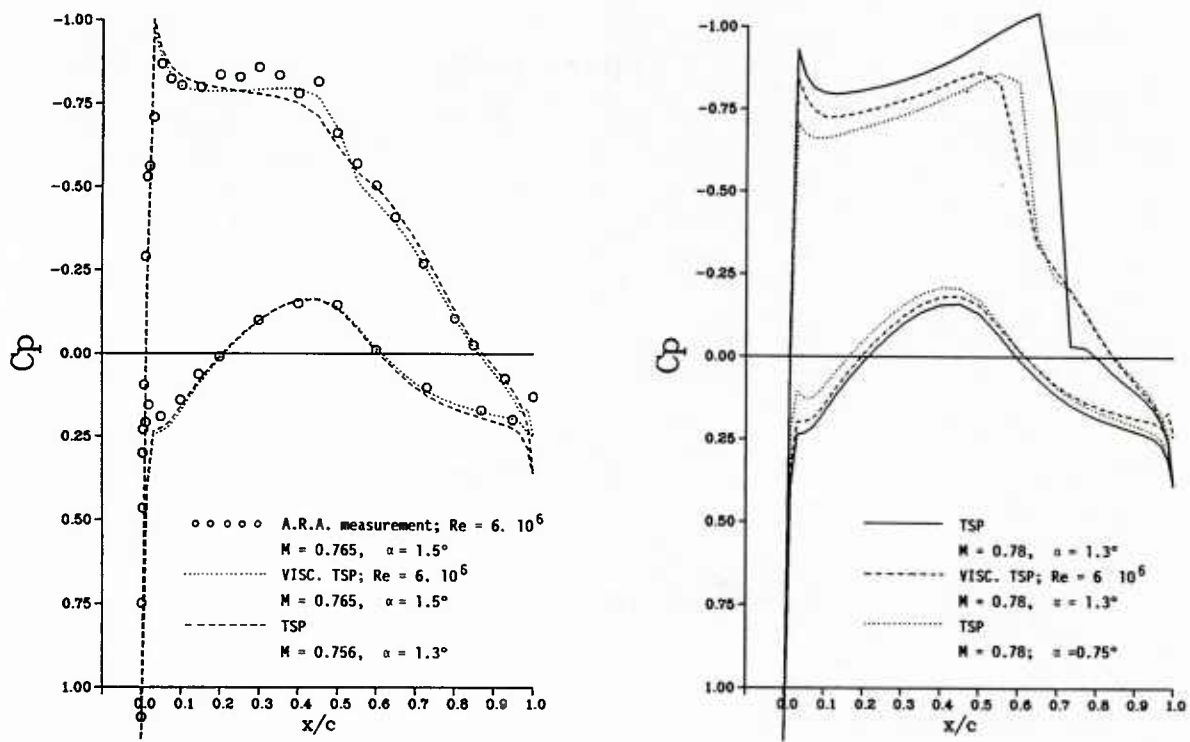
Fig. 6 Steady pressure distribution
MBB–A3 (design conditions)
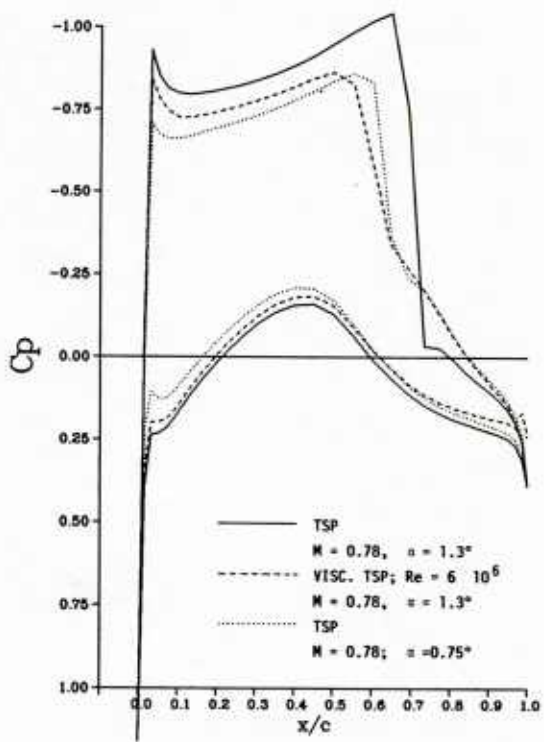
Fig. 7 Steady pressure distribution
MBB–A3 (M=0.78)

Fig. 9 Unsteady pressures, (pitch motion)
calculated with visc. TSP
M=0.756, α=1.3° and Re= 6. 10⁶
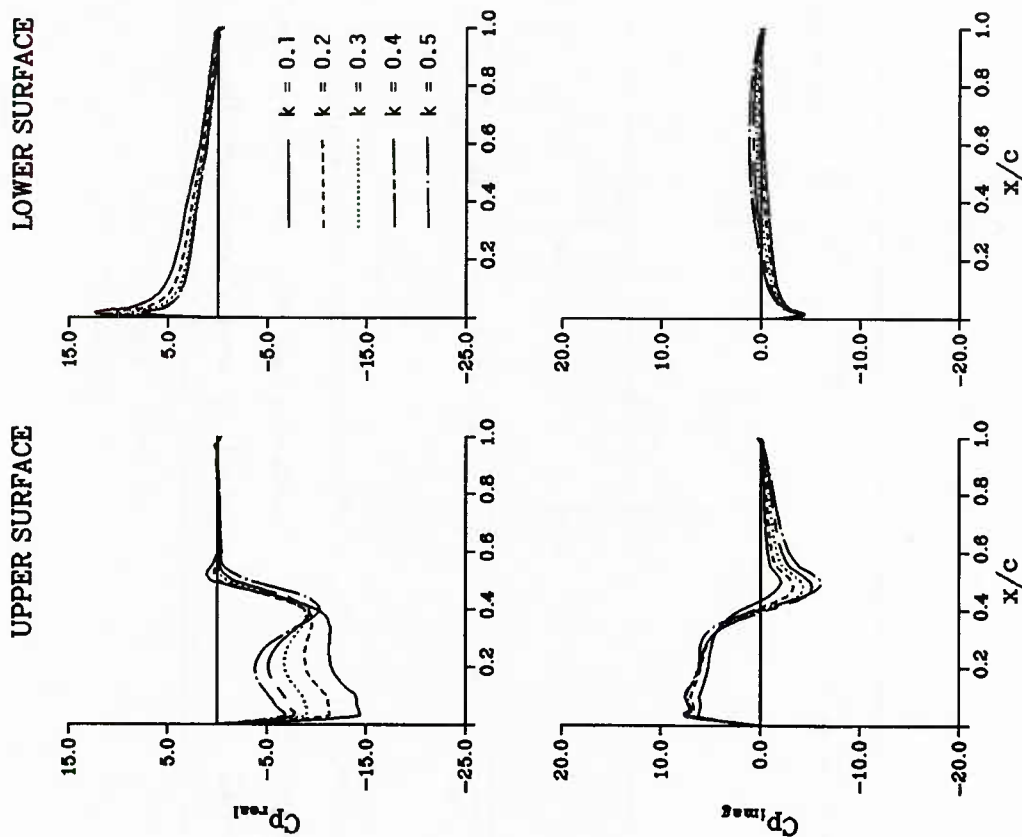
Fig. 8 Unsteady pressures, (pitch motion)
calculated with TSP
M=0.756, α=1.3°
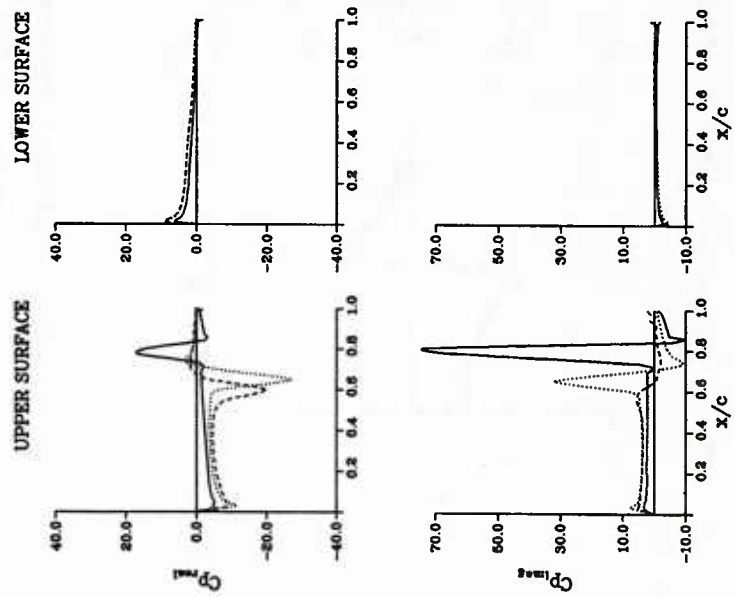
Fig. 10 Unsteady pressures, pitch motion
calculated with TSP and visc. TSP
M=0.78, k=0.2

—————— TSP   M = 0.78,   α = 1.3°
— — — — VISC. TSP M = 0.78,   α = 1.3°
.... TSP   M = 0.78,   α = 0.75°
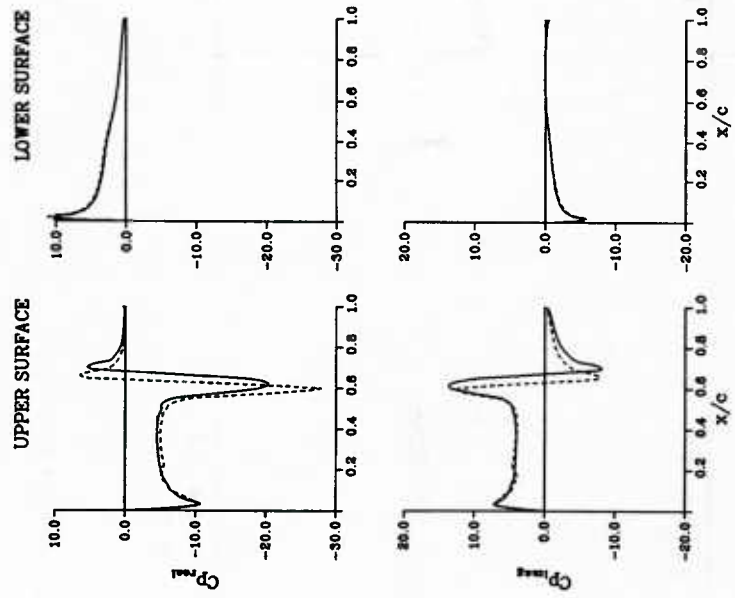
Fig. 11 Unsteady pressures, pitch motion
calculated with Lin. TSP and TSP
M=0.78, α=0.5° and k=0.2

—————— TSP
— — — — LIN. TSP
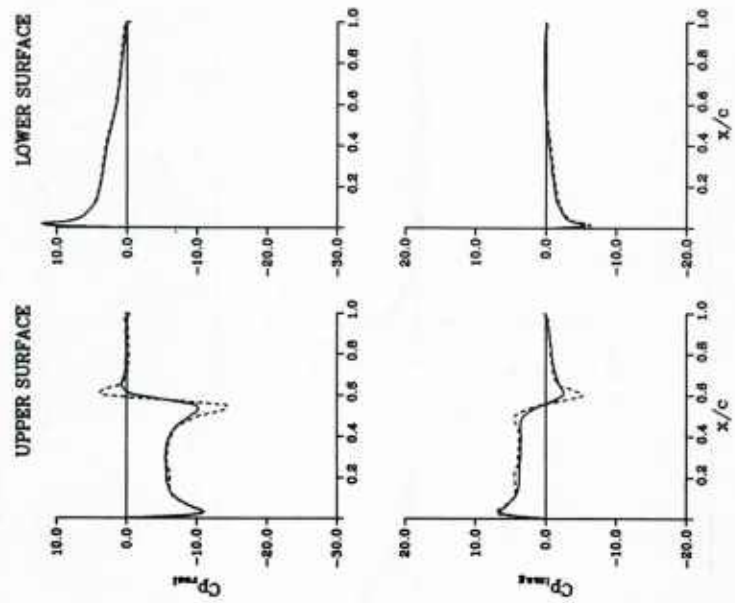
Fig. 12 Unsteady pressures, pitch motion
calculated with visc. Lin. TSP and visc. TSP
M = 0.78, α=0.5°, k=0.2 and Re= 6. 10⁶

—————— VISC. TSP
— — — — VISC. LIN. TSP

- D. L.
- Plate
- LIN. TSP
- TSP
- VISC. LIN. TSP
- VISC. TSP
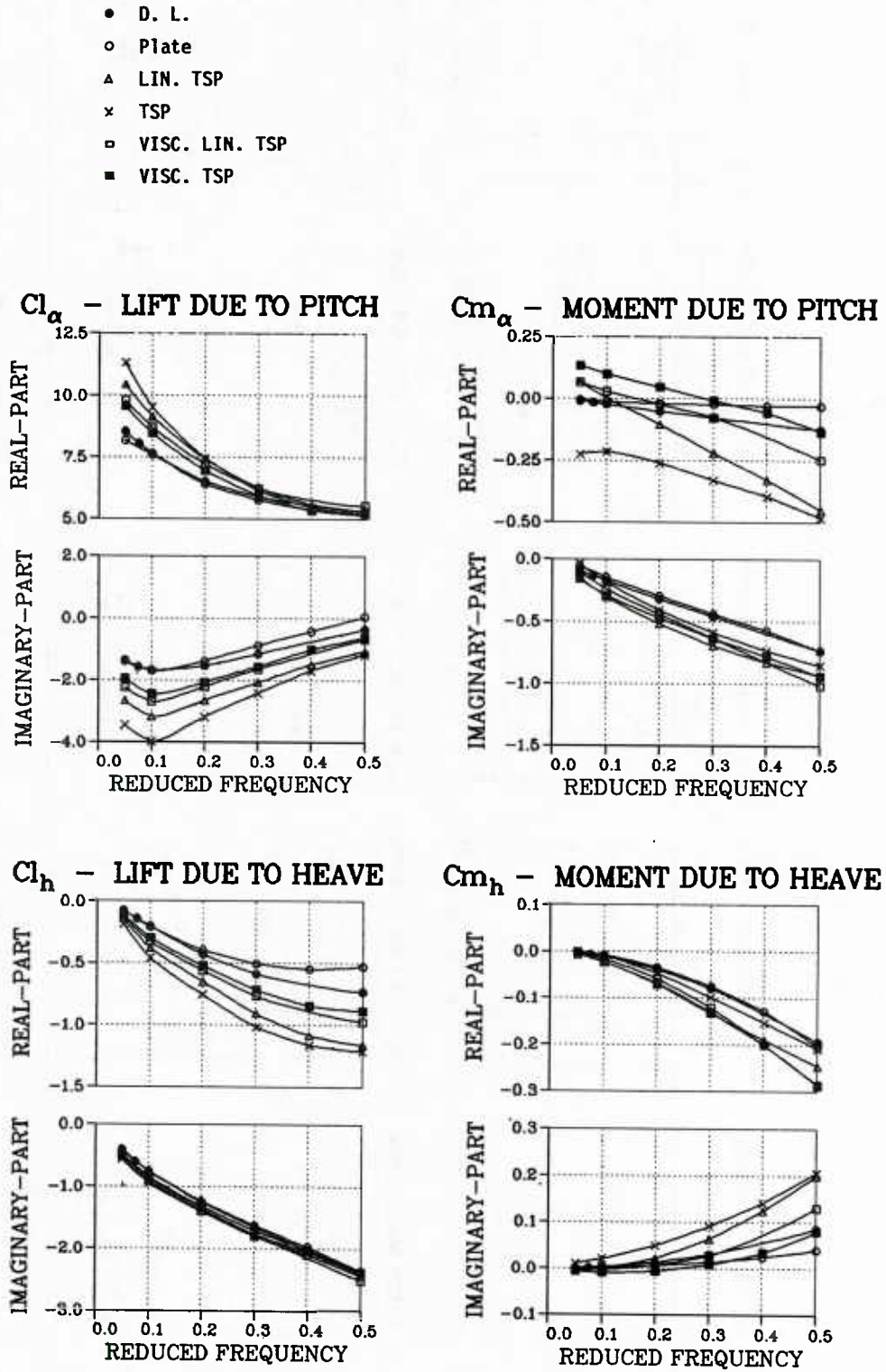
Fig. 13 Unsteady aerodynamic coefficients for

$M = 0.756$ and $\alpha = 1.3°$ (Re=6. 10^6)

● TSP........ α = 0.0°
○ TSP........ α = 0.5°
▲ TSP........ α = 0.75°
✕ VISC. TSP. α = 0.75°

● TSP........ α = 0.0°
○ TSP........ α = 0.75°
▲ TSP........ α = 1.3°
✕ VISC. TSP. α = 1.3°

● TSP........ α = 0.0°
○ TSP........ α = 0.5°
▲ TSP........ α = 0.75°
✕ VISC. TSP. α = 0.75°

Fig. 16 Unsteady aerodynamic coefficients
M=0.8 and α=0° ; 0.5° ; 0.75°

Fig. 15 Unsteady aerodynamic coefficients
M=0.78 and α=0° ; 0.75° ; 1.3°
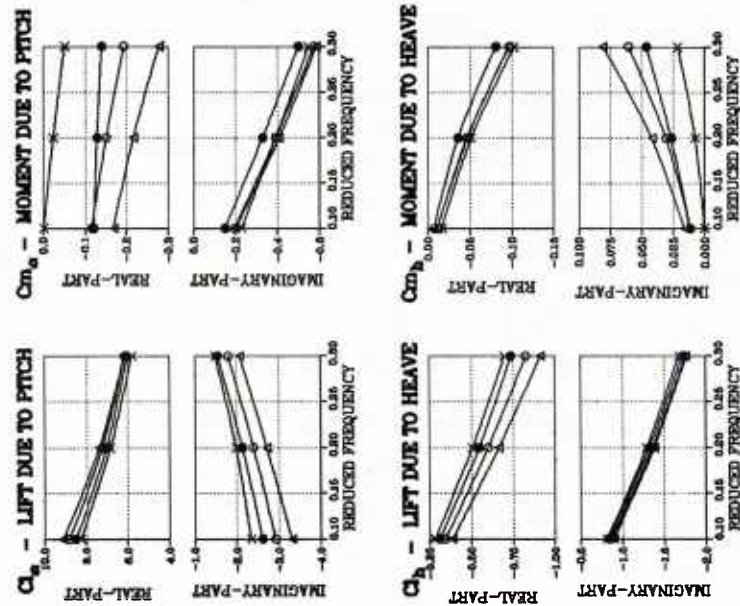
Fig. 14 Unsteady aerodynamic coefficients
M=0.765 and α=0° ; 0.5° ; 0.75°

MODE 1

$h_1^{\frac{1}{4}} = 1$

$\alpha_1 = -0,1$

$f_1 = 10\,Hz$

$X_1^K = \dfrac{h^{\frac{1}{4}}}{\alpha}$
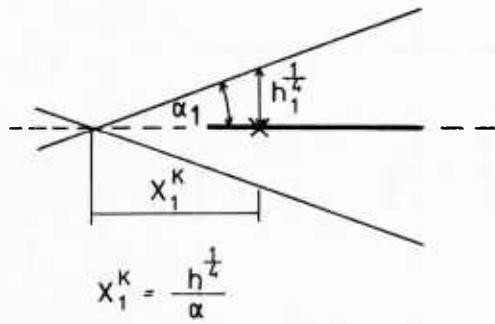
MODE 2
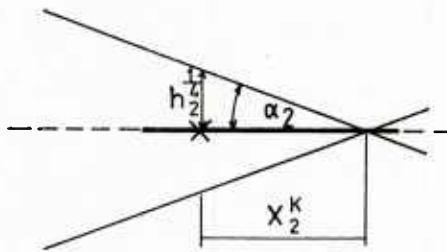
$h_2^{\frac{1}{4}} = 0,5$

$\alpha_2 = 1$

$f_2 = 30\,Hz$

Fig. 17 Dynamic model of a typical section

FLUTTER CALCULATION

● — DOUBLET LATTICE
○ — α = 0.50° LIN.VISC.TSP
△ — α = 0.00° VISC.TSP
× — α = 0.50° VISC.TSP
□ — α = 0.75° VISC.TSP
■ — α = 1.30° VISC.TSP
✕ — α = 0.00° LIN.TSP
▨ — α = 0.50° LIN.TSP
◆ — α = 1.30° LIN.TSP
+ — α =-1.00° TSP
◇ — α = 0.00° TSP
▽ — α = 0.50° TSP
⊕ — α = 0.75° TSP
✻ — α = 1.30° TSP

FLUTTER SIMULATION
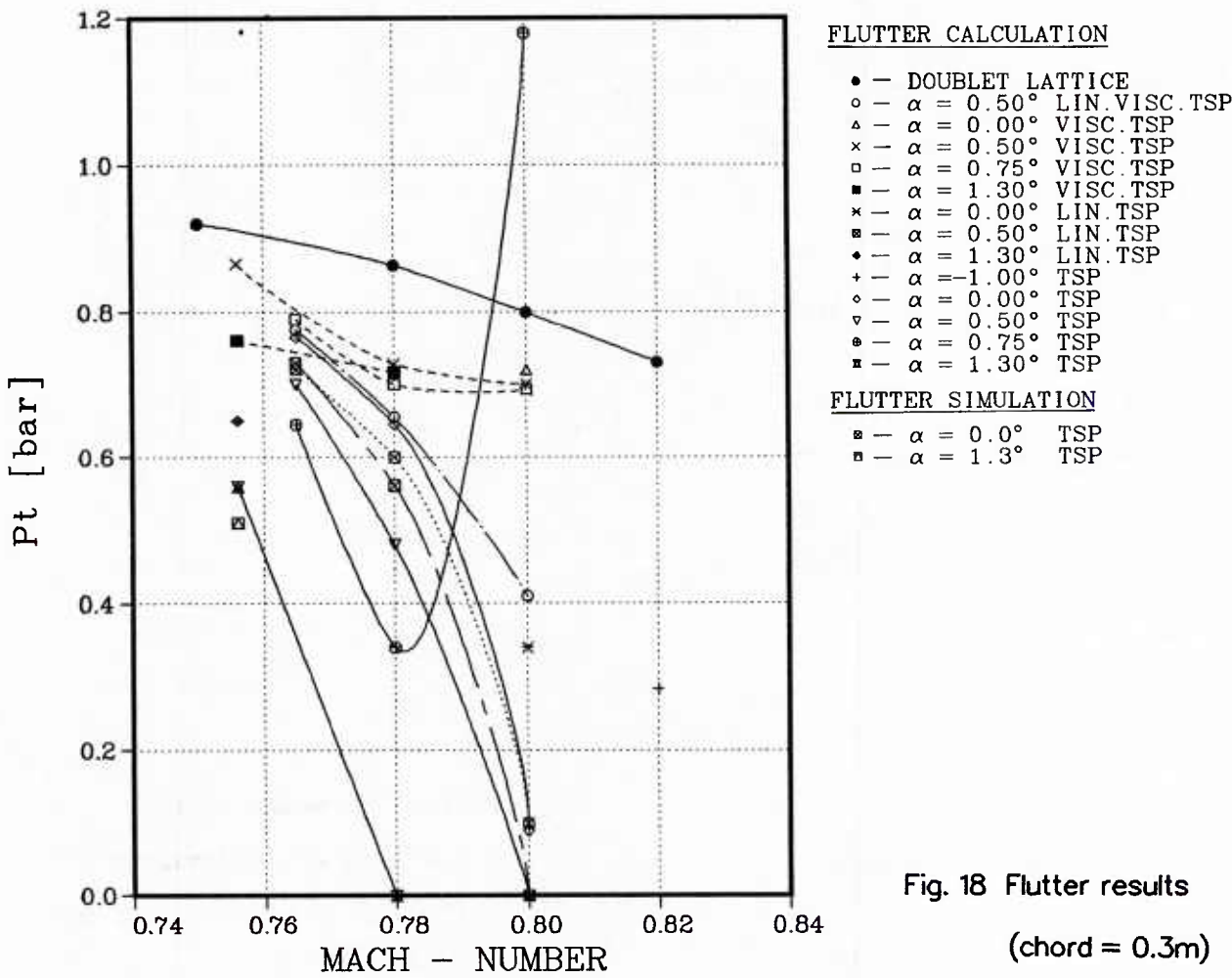
▨ — α = 0.0° TSP
▫ — α = 1.3° TSP

Fig. 18 Flutter results

(chord = 0.3m)
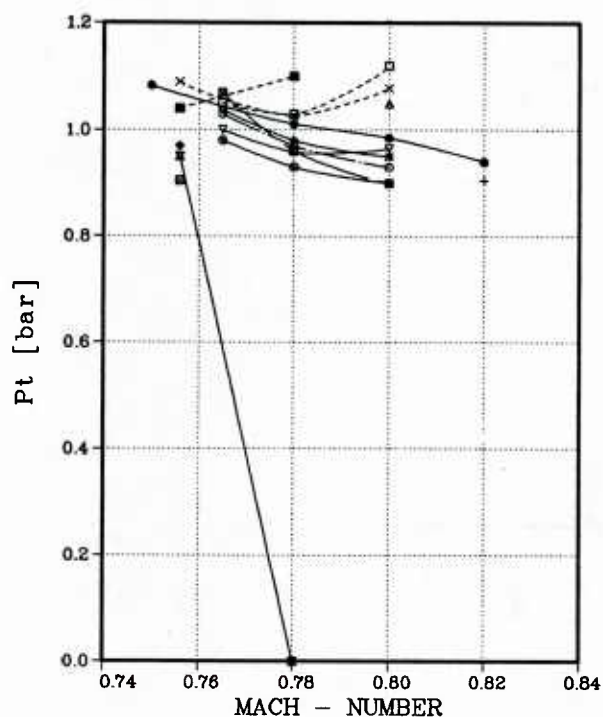
Fig. 19 Flutter results (chord = 0.6m)

FLUTTER CALCULATION

- • — DOUBLET LATTICE
- ○ — α = 0.50° LIN.VISC.TSP
- △ — α = 0.00° VISC.TSP
- × — α = 0.50° VISC.TSP
- □ — α = 0.75° VISC.TSP
- ■ — α = 1.30° VISC.TSP
- ✕ — α = 0.00° LIN.TSP
- ⊞ — α = 0.50° LIN.TSP
- ◆ — α = 1.30° LIN.TSP
- + — α =-1.00° TSP
- ◇ — α = 0.00° TSP
- ▽ — α = 0.50° TSP
- ⊕ — α = 0.75° TSP
- ⊠ — α = 1.30° TSP

FLUTTER SIMULATION

- ⊞ — α = 1.3° TSP
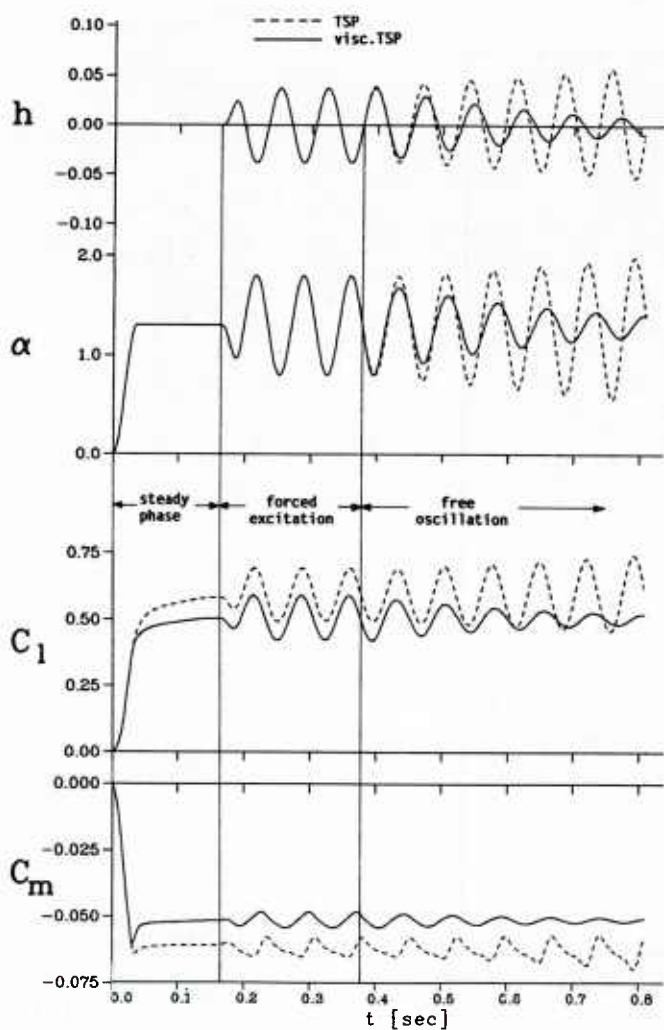
Fig. 20 Flutter simulation results
calculated with TSP and visc. TSP
M=0.756, α=1.3°, P_t =0.55 bar
(chord = 0.3m)
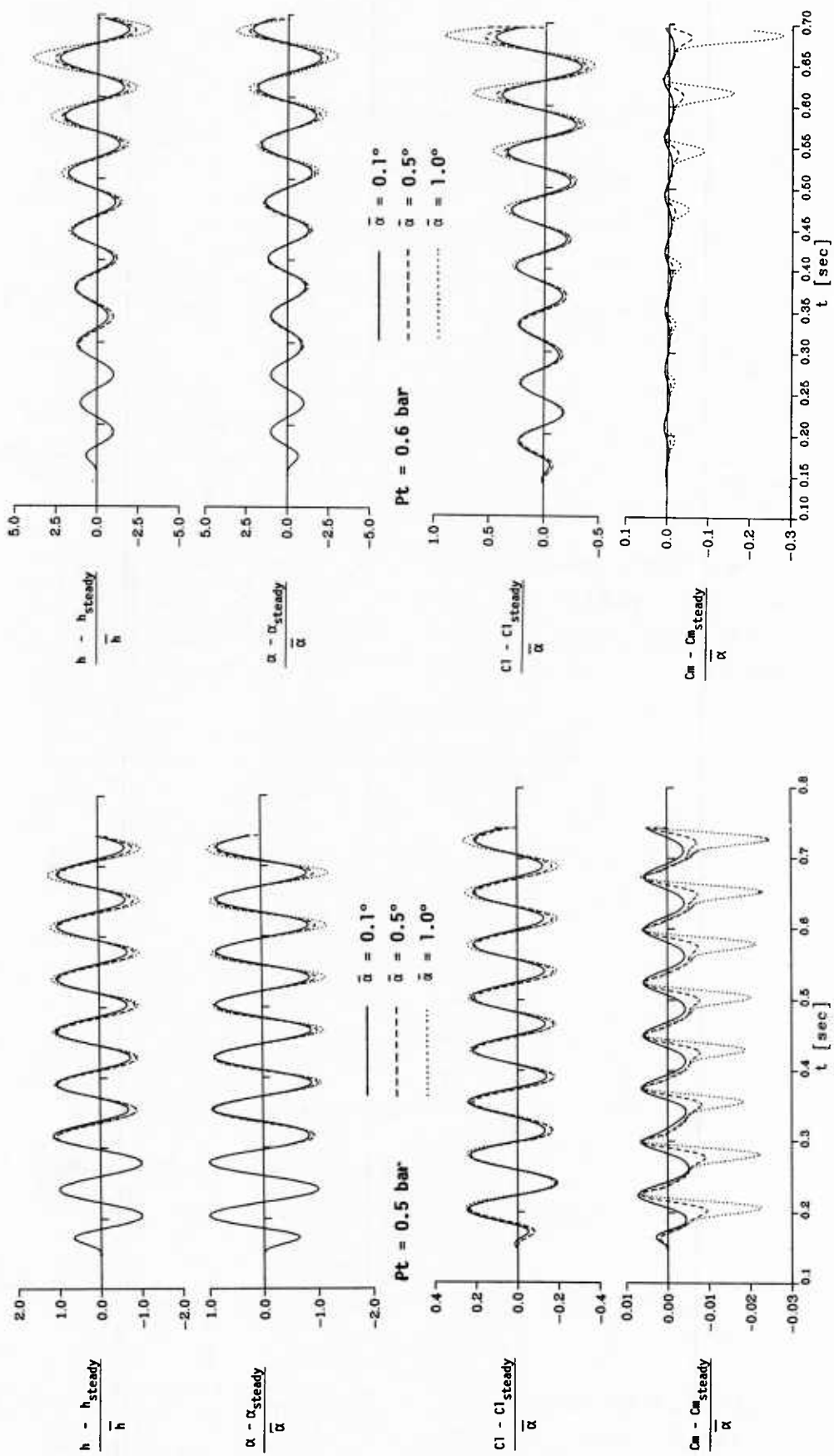
Fig. 21 Flutter simulation results (chord = 0.3m) M=0.756, α=1.3,°
calculated with TSP
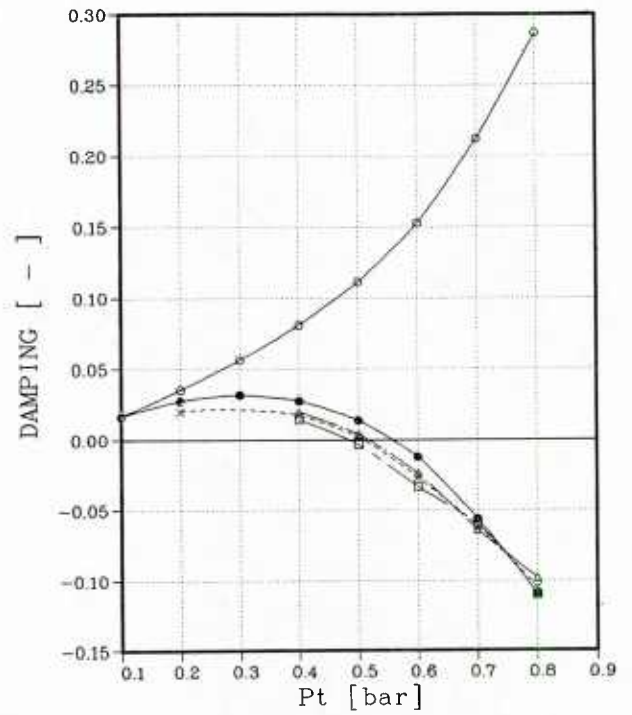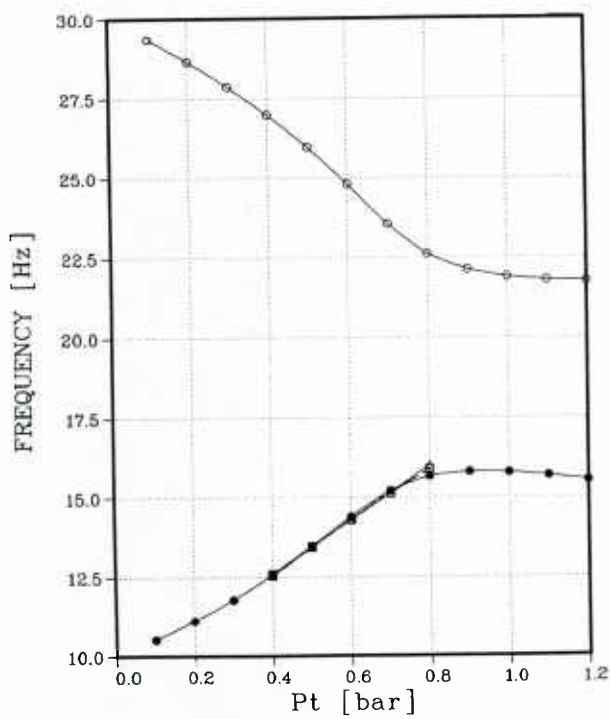
Fig. 22 Comparison between flutter calculation
and flutter simulation results
(chord = 0.3m) M=0.756, α= 1.3^0
calculated with TSP

```
• =    FLUTTER  CALCULATION  1.MODE
o =    FLUTTER  CALCULATION  2.MODE
△ =    FLUTTER  SIMULATION   ᾱ=0.1°
× =    FLUTTER  SIMULATION   ᾱ=0.5°
□ =    FLUTTER  SIMULATION   ᾱ=1.0°
```
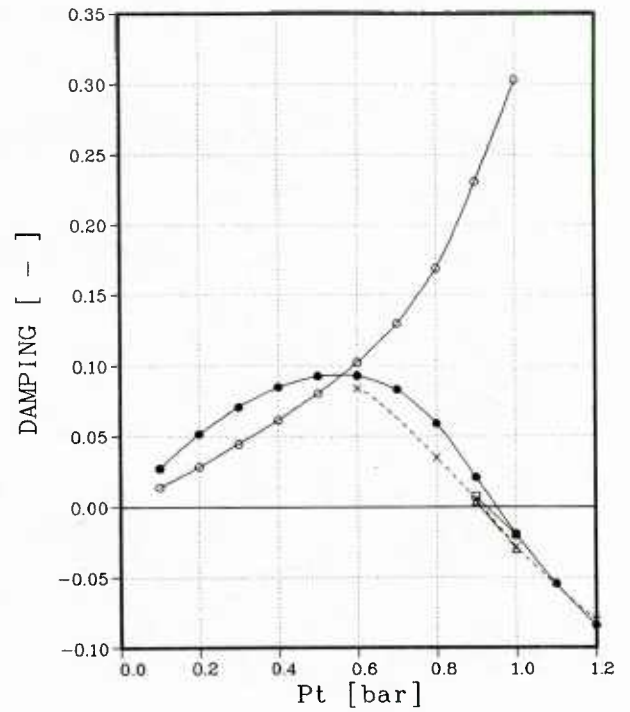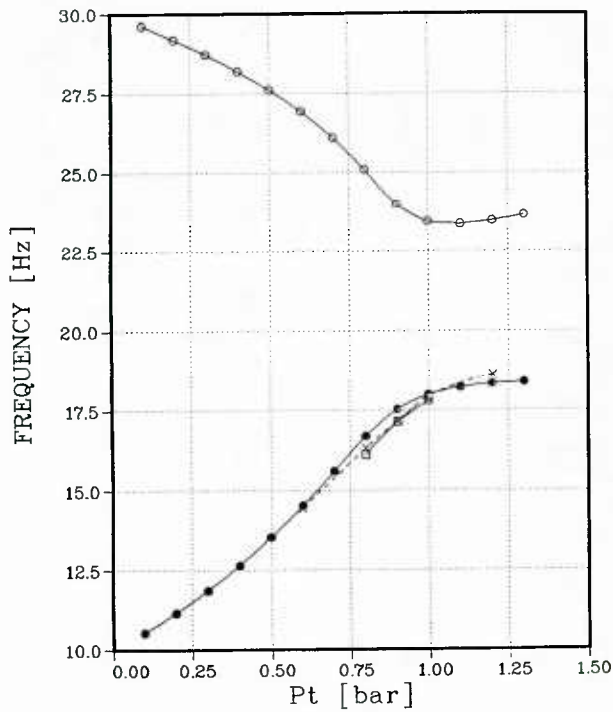

Fig. 23 Comparison between flutter calculation
and flutter simulation results
(chord = 0.6m) M=0.756, α= 1.3^0
calculated with TSP

```
• =    FLUTTER  CALCULATION  1.MODE
o =    FLUTTER  CALCULATION  2.MODE
△ =    FLUTTER  SIMULATION   ᾱ=0.1°
× =    FLUTTER  SIMULATION   ᾱ=0.5°
□ =    FLUTTER  SIMULATION   ᾱ=1.0°
```

AGARD Report No.749 Advisory Group for Aerospace Research and Development, NATO FUTURE RESEAR ON TRANSONIC UNSTEADY AERODYNAMICS AND ITS AEROELASTIC APPLICATIONS Published August 1987 44 pages This Workshop focused on strategies for promoting and developing engineering-level transonic flutter prediction techniques. The technology of transonic aerodynamics is currently undergoing rapid development. Significant progress is being made to solve the inherently nonlinear equations P.T.O	AGARD-R-749 Transonic characteristics Unsteady state Aerodynamics Flutter Mathematical prediction Aeroelasticity	AGARD Report No.749 Advisory Group for Aerospace Research and Development, NATO FUTURE RESEAR ON TRANSONIC UNSTEADY AERODYNAMICS AND ITS AEROELASTIC APPLICATIONS Published August 1987 44 pages This Workshop focused on strategies for promoting and developing engineering-level transonic flutter prediction techniques. The technology of transonic aerodynamics is currently undergoing rapid development. Significant progress is being made to solve the inherently nonlinear equations P.T.O	AGARD-R-749 Transonic characteristics Unsteady state Aerodynamics Flutter Mathematical prediction Aeroelasticity
AGARD Report No.749 Advisory Group for Aerospace Research and Development, NATO FUTURE RESEAR ON TRANSONIC UNSTEADY AERODYNAMICS AND ITS AEROELASTIC APPLICATIONS Published August 1987 44 pages This Workshop focused on strategies for promoting and developing engineering-level transonic flutter prediction techniques. The technology of transonic aerodynamics is currently undergoing rapid development. Significant progress is being made to solve the inherently nonlinear equations P.T.O	AGARD-R-749 Transonic characteristics Unsteady state Aerodynamics Flutter Mathematical prediction Aeroelasticity	AGARD Report No.749 Advisory Group for Aerospace Research and Development, NATO FUTURE RESEAR ON TRANSONIC UNSTEADY AERODYNAMICS AND ITS AEROELASTIC APPLICATIONS Published August 1987 44 pages This Workshop focused on strategies for promoting and developing engineering-level transonic flutter prediction techniques. The technology of transonic aerodynamics is currently undergoing rapid development. Significant progress is being made to solve the inherently nonlinear equations P.T.O	AGARD-R-749 Transonic characteristics Unsteady state Aerodynamics Flutter Mathematical prediction Aeroelasticity

describing unsteady motions of wings in transonic flow, while the availability of reliable and efficient computational methods will greatly enhance the ability to predict the aeroelastic behaviour of modern aircraft operating under transonic flow conditions.

AGARD-SMP has previously coordinated unsteady aerodynamic research carried out on a number of "standard" wind tunnel model configurations and published the results. The proposals contained in the Evaluation Report (W.J.Mykytow) on the Fall 1984 Structures and Materials Panel Specialists' Meeting on "Transonic Unsteady Aerodynamics", together with an expanded range of aeroelastic configurations, formed the guidelines which this Workshop followed.

Two of the keynote papers presented at this Workshop are published in this Report.

Papers presented at the 63rd Meeting of the Structures and Materials Panel of AGARD, in Athens, Greece, 28 September—3 October 1986.

ISBN 92-835-0425-9

U230890

**DISTRIBUTION OF UNCLASSIFIED
AGARD PUBLICATIONS**

AGARD does NOT hold stocks of AGARD publications at the above address for general distribution. Initial distribution of AGARD publications is made to AGARD Member Nations through the following National Distribution Centres.Further copies are sometimes available from these Centres, but if not may be purchased in Microfiche or Photocopy form from the Purchase Agencies listed below.

NATIONAL DISTRIBUTION CENTRES

BELGIUM
Coordonnateur AGARD — VSL
Etat-Major de la Force Aérienne
Quartier Reine Elisabeth
Rue d'Evere, 1140 Bruxelles

CANADA
Defence Scientific Information Services
Dept of National Defence
Ottawa, Ontario K1A 0K2

DENMARK
Danish Defence Research Board
Ved Idraetsparken 4
2100 Copenhagen Ø

FRANCE
O.N.E.R.A. (Direction)
29 Avenue de la Division Leclerc
92320 Châtillon

GERMANY
Fachinformationszentrum Energie,
Physik, Mathematik GmbH
Kernforschungszentrum
D-7514 Eggenstein-Leopoldshafen

GREECE
Hellenic Air Force General Staff
Research and Development Directorate
Holargos, Athens

ICELAND
Director of Aviation
c/o Flugrad
Reyjavik

ITALY
Aeronautica Militare
Ufficio del Delegato Nazionale all'AGARD
3 Piazzale Adenauer
00144 Roma/EUR

LUXEMBOURG
See Belgium

NETHERLANDS
Netherlands Delegation to AGARD
National Aerospace Laboratory, NLR
P.O. Box 126
2600 AC Delft

NORWAY
Norwegian Defence Research Establishment
Attn: Biblioteket
P.O. Box 25
N-2007 Kjeller

PORTUGAL
Portuguese National Coordinator to AGARD
Gabinete de Estudos e Programas
CLAFA
Base de Alfragide
Alfragide
2700 Amadora

TURKEY
Milli Savunma Bakanlığı
ARGE Daire Başkanlığı
Ankara

UNITED KINGDOM
Defence Research Information Centre
Kentigern House
65 Brown Street
Glasgow G2 8EX

UNITED STATES
National Aeronautics and Space Administration (NASA)
Langley Research Center
M/S 180
Hampton, Virginia 23665

THE UNITED STATES NATIONAL DISTRIBUTION CENTRE (NASA) DOES NOT HOLD
STOCKS OF AGARD PUBLICATIONS, AND APPLICATIONS FOR COPIES SHOULD BE MADE
DIRECT TO THE NATIONAL TECHNICAL INFORMATION SERVICE (NTIS) AT THE ADDRESS BELOW.

PURCHASE AGENCIES

National Technical
Information Service (NTIS)
5285 Port Royal Road
Springfield
Virginia 22161, USA

ESA/Information Retrieval Service
European Space Agency
10, rue Mario Nikis
75015 Paris, France

The British Library
Document Supply Division
Boston Spa, Wetherby
West Yorkshire LS23 7BQ
England

Requests for microfiche or photocopies of AGARD documents should include the AGARD serial number, title, author or editor, and publication date. Requests to NTIS should include the NASA accession report number. Full bibliographical references and abstracts of AGARD publications are given in the following journals:

Scientific and Technical Aerospace Reports (STAR)
published by NASA Scientific and Technical
Information Branch
NASA Headquarters (NIT-40)
Washington D.C. 20546, USA

Government Reports Announcements (GRA)
published by the National Technical
Information Services, Springfield
Virginia 22161, USA

SPS

*Printed by Specialised Printing Services Limited
40 Chigwell Lane, Loughton, Essex IG10 3TZ*

ISBN 92-835-0425-9